

INVESTIGATION OF BOUNDARY LAYER AND
PERFORMANCE EFFECTS OF TRANSPERSION COOLING
THROUGH A POROUS PLATE IN A ROCKET NOZZLE

THESIS

David N. Keener, Second Lieutenant, USAF

AFIT/GA/ENY/94D-3

This document has been approved
for public release and sale; its
distribution is unlimited.

DEPARTMENT OF THE AIR FORCE
AIR UNIVERSITY
AIR FORCE INSTITUTE OF TECHNOLOGY

Wright-Patterson Air Force Base, Ohio



Accesion No.	<i>1</i>
NTIS Catalog No.	<i>1</i>
DTIC Type	<i>1</i>
Unannounced	<input checked="" type="checkbox"/>
Justification	<i>1</i>
By	<i>1</i>
Distribution /	<i>1</i>

A-1

**INVESTIGATION OF BOUNDARY LAYER AND
PERFORMANCE EFFECTS OF TRANSPERSION COOLING
THROUGH A POROUS PLATE IN A ROCKET NOZZLE**

THESIS

David N. Keener, Second Lieutenant, USAF

AFIT/GA/ENY/94D-3

19950103 054

19950103 054

Approved for public release; distribution unlimited

INVESTIGATION OF BOUNDARY LAYER AND
PERFORMANCE EFFECTS OF TRANSPIRATION COOLING
THROUGH A POROUS PLATE IN A ROCKET NOZZLE

THESIS

Presented to the Faculty of the Graduate School of Engineering

of the Air Force Institute of Technology

Air University

In Partial Fulfillment of the
Requirements for the Degree of
Master of Science in Astronautical Engineering

David N. Keener, B.S.

Second Lieutenant, USAF

December 1994

Approved for public release; distribution unlimited

INVESTIGATION OF BOUNDARY LAYER AND
PERFORMANCE EFFECTS OF TRANSPERSION COOLING
THROUGH A POROUS PLATE IN A ROCKET NOZZLE

THESIS

Presented to the Faculty of the Graduate School of Engineering

of the Air Force Institute of Technology

Air University

In Partial Fulfillment of the

Requirements for the Degree of

Master of Science in Astronautical Engineering

David N. Keener, B.S.

Second Lieutenant, USAF

December 1994

Approved for public release; distribution unlimited

Preface

This investigation brings the AFIT Low Speed Shock Tube back into use on a study of the effects of transpiration cooling on the boundary layer in a Mach 2.0 nozzle. The experiment was performed in parallel with a heat transfer reduction study carried out using the same equipment. The focus of the study was characterizing the effects that the increased boundary layer thickness had on the performance of the nozzle in terms of boundary layer displacement thickness and exit Mach number. This is the first in a new series of experiments that are to be run on this nozzle, and a great amount of headway has been made during the course of this project. That headway would not have been possible, however, without the help of several people.

Many thanks go out to my advisor, Dr. Rodney Bowersox, and Lt Col Jerry Bowman for their knowledge of the subject, the wide berth allowed me to perform my work, and answers to all my questions. Thanks and appreciation go to Mr. Tim Hancock of the AFIT Machine Shop for his excellent work on the model. He was asked to do many unfamiliar things and did so with professionalism, creativity, and precision. Also, Mr. Andy Pitts and the other members of the AFIT/ENY Laboratory Staff receive thanks for helping with all the hardware concerns surrounding this project. Special thanks goes to Andy for his help in setting up the timing circuit that allowed me great success at taking shadowgraphs.

I enjoyed my time working in Rm.146, and will take all the things I have learned from all of you and hopefully put them to good use at my next assignment and beyond.

David N. Keener

Table of Contents

	Page
Preface	ii
List of Figures	v
List of Tables	vii
List of Symbols	viii
Abstract	xi
I. Introduction	1
1.1 Background	1
1.2 Problem	4
1.3 Summary of Current Knowledge	5
1.4 Objectives and Scope	11
1.5 Methodology	11
II. Theory	14
2.1 Turbulent Boundary Layer	14
2.2 Transpired Boundary Layer	23
III. Experimental Setup and Procedures	25
3.1 Shock Tube Configuration	25
3.2 Test Article	27
3.2.1 General Description	27
3.2.2 Nozzle Design Tools	31
3.3 Instrumentation and Data Collection	31
3.4 Shadowgraph Flow Visualization	32
3.5 Procedural Notes	38
IV. Results and Discussion	40
4.1 Baseline Results	40
4.1.1 Actual Test Conditions	40
4.1.2 Characterization of the Flow Field	41
4.1.3 Non Blowing vs Blowing Side	43

4.1.4 Exit Mach Number Profile	46
4.2 Blowing Cases	49
4.2.1 Definition	49
4.2.2 Boundary Layer Growth	50
4.2.3 Wall Mach Number	54
4.3 Performance	56
4.3.1 Exit Mach Number	56
4.3.2 Specific Impulse	62
V. Conclusions and Recommendations	65
APPENDIX A: Gamma Calculation for air/He driver	A.1
APPENDIX B: Computer Resources	B.1
APPENDIX C: Calibration Data	C.1
APPENDIX D: Procedures	D.1
APPENDIX E: Throat Boundary Layer Thickness Calculations	E.1
APPENDIX F: Porous Material Selection	F.1
Bibliography	Bib.1
Vita	Vita.1

List of Figures

Figure	Page
1.1 Boundary Layer Growth w/ Blowing (Schetz, 1984:205)	6
1.2 Boundary Layer Thickness w/ Helium Injection (Schetz, 1984:276)	6
1.3 Flat Plate Boundary Layer Growth w/ Injection (Goldstein, 1965:356)	8
1.4 Thrust Losses w/ Film Cooling in a Nozzle (Azevedo, 1993:48)	9
2.1 Control Volume (Hill and Peterson:1992:102)	15
3.1 Shock Tube Configuration	26
3.2 Nozzle Design w/ Dimensions	28
3.3 Tripped Flow at Porous Material/Aluminum Seam	30
3.4 Shadowgraph Setup	33
3.5 Pitot Probe Bent Out of Flow	34
3.6 Timing Circuit Block Diagram	35
3.7 Schematic of Voltage Divider Circuit	38
4.1 Characterization of Flow Dynamics	42
4.2 Thickness vs Distance From Throat for Baseline Case	44
4.3 Baseline Exit Mach Number Profile	47
4.4 Pitot Probe as Part of the Wall	48
4.5 Shadowgraphs Showing Boundary Layer at Each Blowing Ratio	51
4.6 Blowing Ratio vs Boundary Layer Growth	53
4.7 Boundary Layer Growth vs Distance from Throat	54
4.8 Mach Number vs. Distance from Throat	55

4.9	Pressure Ratio vs. Distance from Throat	56
4.10	Comparing Blowing and Non Blowing Mach Number Profiles	58
4.11	Exit Mach Number Trends vs Blowing Ratio	61
4.12	Decrease in Uniformity w/ Blowing	61
4.13	Blowing Ratio vs Isp	63
4.14	Blowing Ratio vs Thrust and Mass Flow Rate	64

List of Tables

Table		Page
3.1	Summary of Expected Test Conditions	27
3.2	Timing Circuit Elements w/ Function	35
4.1	Summary of Actual Test Conditions	40
4.2	Comparing Non Blowing and Blowing Sides of Nozzle	44
4.3	Summary of Baseline Exit Mach Number Data	46
4.4	Summary of Blowing Conditions	50
4.5	Summary of Blowing Ratio and each Blowing Level	50
4.6	Summary of Boundary Layer Growth Data	52
4.7	Summary of Exit Mach Number Data	57

List of Symbols

<u>Symbol</u>	<u>Description</u>	<u>Units</u>
\dot{m}_i	Injected mass flow rate	kg/sec
\dot{m}_∞	Freestream mass flow rate	kg/sec
\dot{m}''	Mass flow rate through porous material	kg/sec
δ	Boundary layer thickness	mm
δ^*	Displacement thickness	mm
θ	Momentum thickness	mm
H	Ratio: θ / δ^*	
C_f	Coefficient of friction	
C_v	Thrust efficiency (T_{act}/T_{id})	
ΔC_v	Change in thrust efficiency	
B	Blowing ratio	
s	Arc length along porous area	cm (in)
ρ	Gas density	kg/m ³
ρ^*	Density of gas at throat	kg/m ³
u	Gas velocity	m/s
u^*	Velocity of gas at throat	m/s
γ	Ratio of specific heats (c_p/c_v)	
A	Nozzle area at arbitrary point	m ²
A^*	Throat area	m ²
M_e	Exit Mach number	

Δp	Pressure drop across porous material	Pa
h	Indefinitely large distance from nozzle wall, limit of integration	m
U	Freestream velocity	m/s
τ_0	Wall shear stress	Pa
τ_l	Local wall shear stress	Pa
y_l	Some position away from wall	m
R	Radius of channel	m
ν	Kinematic viscosity (μ / ρ)	m^3/s
Re_δ	Local Reynolds number	
Re^*	Throat Reynolds number	
k^+	Roughness Reynolds number	
κ	0.41	
B	Outer variable constant (5.0)	
Π	Cole's wake parameter	
A	Inner variable constant (dependent on pressure gradient present)	
u^+	Nondimensional velocity in turbulent shear layer	
v^+	Nondimensional normal velocity at wall	
λ	Nondimensional boundary layer parameter	
Z	Nondimensional boundary layer parameter	
C_D	Discharge coefficient	
R_c	Throat radius of curvature	m
R^*	Radius of throat	m

TD _t	Total time delay	μs
TD ₄₃₆	Cordin Proportional Delay Generator delay time	μs
TD ₄₅₃	Cordin Delay Generator delay time	μs
x	horizontal distance along nozzle	cm (in)
i	Subscript indicating injected gas condition	
∞	Subscript indicating freestream gas condition	
p	Subscript indicating plenum gas condition	

Abstract

The effects of transpiration cooling through a porous wall on nozzle performance was investigated. The experiments were performed in the AFIT Low Pressure shock tunnel. The tunnel was fitted with a two dimensional, Mach 2.0 characteristic nozzle with one wall constructed of porous material. Blowing ratios from 0.4%-1.2% of the mainstream flow were studied. This study extends current flat plate knowledge of transpiration cooling by including compressibility and a severe favorable pressure gradient.

Boundary layer growth as a result of the transpiration was measured using flow visualization, and the effect of that growth on the exit Mach number profile was investigated. Analysis of experimental data showed increases of up to 47% in boundary layer thickness with transpiration, and because the blowing ratios used in this experiment were very low due to equipment constraints, the resulting trends show no sign of leveling off leaving much room for continued research of this kind at higher blowing ratios. The results do, however, show that performance losses due to transpiration are such that transpiration may be a viable nozzle cooling method even up to high blowing ratios without having large adverse effects on performance.

This study, taken together, with a parallel study on heat transfer reduction using the same equipment endeavors to begin to characterize the tradeoff between the performance gain due to heat transfer reduction and the loss due to boundary layer growth in a transpiration cooled nozzle. Defining the optimal blowing ratio to minimize heat transfer and optimize performance would be the final goal of such an effort.

INVESTIGATION OF BOUNDARY LAYER AND PERFORMANCE EFFECTS OF TRANSPERSION COOLING THROUGH A POROUS PLATE ON A ROCKET NOZZLE

I. Introduction

1.1 Background

Currently there are quality rocket engine systems and high temperature wind tunnel facilities in use. Further improvements in the performance of these systems requires higher operating temperatures. A problem is that, without cooling, operating at higher temperatures tends to compromise the structural integrity of the thrust chamber. For example, in hypersonic wind tunnels, for example, erosion of the tunnel wall sometimes occurs due to high operating temperatures. Erosion can cause debris to travel down the tunnel that often breaks expensive test articles because of impact speeds. Nozzle heat transfer and material thermal limitations, then, remain a limiting factor in the performance of modern rocket engines. Therefore, heat transfer reduction is the key to improving the efficiency structural integrity of rocket systems, but the relationship between heat transfer and the boundary layer present in the flow field is also very important.

Heat transfer and boundary layer thickness in a nozzle are inversely related phenomena (Hill and Peterson,1992:544). The boundary layer thickness has been demonstrated analytically by Bartz (1955:1243) to be a minimum at the throat of a supersonic nozzle. In addition, its thickness at the throat is not highly dependent on its thickness before the throat or the rate of convergence of the nozzle after the throat (Hill and Peterson,1992:545). This means that in

virtually every case, the boundary layer thickness will be a minimum at the throat of a nozzle, and this is a very important point in relation to heat transfer.

A turbulent boundary layer provides insulation to nozzle walls that makes heat transfer to the walls less than if no boundary layer were present. The thicker the boundary layer, the more insulation it provides, and the lower the heat transfer through it. This is the inverse relationship mentioned above, and it implies that heat transfer will be greatest in a rocket nozzle at the throat because the boundary layer is a minimum there (Hill and Peterson,1992:545). A further implication is that heat transfer will be a maximum at the throat in nearly every case because of throat boundary layer thickness being minimum in nearly every case. This relationship has been validated both analytically and experimentally (Hill and Peterson,1992:551). Actively cooled rocket nozzles allow the high combustion temperatures necessary for high performance while maintaining the structural integrity of the nozzle. Several methods of active cooling have been employed to address this problem, including regenerative, film, and transpiration cooling.

Regenerative cooling involves pumping a liquid through channels surrounding the outside of the combustion chamber. This method has been used extensively because of its relative simplicity and low cost. Also, the heat absorbed by the coolant is not wasted because it augments the initial energy content of the propellant prior to injection, increasing the exhaust velocity slightly (Sutton,1992:290). One drawback to regenerative cooling is the additional pumping requires to force coolant through the coolant lines. This reduces the turbopump's ability to pressurize the combustion chamber and leads to lower expansion ratios and associated lower specific impulses.

Film cooling involves injecting low temperature gas or liquid through one or several discrete holes in the nozzle wall to establish a protective film on the surface. Because the coolant is inside the thrust chamber, it accepts heat directly, which makes it a more effective cooling method than regenerative cooling. It is relatively easy to implement and has been used in thrust chambers for many years (Sutton,1992:294). The drawback of film cooling is that it requires large injection mass flow rate per unit area (10-300% mainstream flow), which can cause thrust losses due to disturbance of the primary flow (Azevedo,1993:44).

Transpiration cooling is essentially the limiting case of film cooling because it involves pushing gas or liquid uniformly through an area of porous wall material (Sutton,1992:294). It can be thought of as an infinite number of film cooling ports with zero distance between them. Though the concept is similar to film cooling, the effects on heat transfer and boundary layer are very different because the fluid enters the flow through the porous material at very low velocity and does not cause as great a disturbance to the flow field. This cooling technique has been successfully used for cooling injector faces on the moon launch vehicle and the Space Shuttle Main Engines, but it has not been used in cooling the thrust chamber or nozzle regions of large rocket engines. Due to the steep pressure gradients along the inner wall of the nozzle, especially near the throat, proper cooling requires a variable porosity and/or thickness wall material. The manufacture of large, complex shapes of porous materials is a difficult problem, and has been a great challenge to transpiration cooling in this region (Sutton, 1992:294).

As mentioned above, transpiration cooling has been used very little in practice, and no generalized analytical relations exist for the prediction of heat flux or boundary layer growth in configurations with pressure gradient, as in the case of supersonic nozzles (Beitel,1993:49). It is

possible that heat transfer rate reduction similar to or better than film cooling can be realized with decreased flow disturbances, indicating that transpiration cooling could be a more attractive method than film or regenerative cooling. Therefore, this investigation proposes to study the effects of transpiration cooling in a supersonic nozzle on boundary layer growth and performance at low blowing ratios.

1.2 Problem

Transpiration cooling has a significant effect on the turbulent boundary layer structure while being a very effective way to protect surface from hot mainstream flow (Kays and Crawford, 1980:179,223). Semiempirical relationships have been developed for predicting the effect of transpiration on turbulent boundary layers over a flat plate, and additional data has been taken to validate these relations. As mentioned above, transpiration cooling has been used very little in practice, and only practical data will show its true benefits. Heat transfer rate reduction with transpiration cooling may be similar to film cooling, and because of decreased flow disturbances, reduced performance loss for the same heat transfer reduction could be achieved. Therefore, transpiration cooling could be an attractive alternative to film, but practical data is needed to show this benefit.

The problem addressed here, then, was the lack of knowledge of the effects of transpiration cooling in supersonic nozzles because data of this type was needed to show how transpiration cooling could improve current rocket systems. Specific parameters that were investigated include boundary layer thickness, exit Mach number, and specific impulse, all of which affect the performance of the nozzle.

1.3 Summary of Current Knowledge

Since the goal of this research was showing the effect of transpiration on boundary layer thickness and performance, previously collected knowledge in each category was desired for comparison. The situation here involved a severe favorable pressure gradient (i.e., a supersonic nozzle), and it appeared that, as Azevedo asserts (1993:43), most studies up to this time had concentrated on the heat transfer aspect of transpiration cooling. In addition, most of those studies used flat plates. There was not a wealth of data available concerning the effects of transpiration cooling on boundary layer growth and even less concerning its effect on nozzle performance, but following is a synopsis of the information collected.

While transpiration cooling has never made it into wide practice, it is not a new idea. Since the 1950s, it has been the subject of research aimed at cooling aerodynamic surfaces subject to high heating (Kays and Moffat, 1975:224). Aerojet has dealt in systems employing porous surfaces since 1946, and in 1967 they fired the Aerojet ARES to demonstrate the technology. This system produced 445 kN (100,000 lb_f) of thrust with a 20.7 MPa (3000 psi) transpiration cooled thrust chamber. Aside from this, however, transpiration cooled thrust chambers are virtually foreign to the commercial rocket industry. Research in the area has continued, and a group at Stanford University collected a large amount of data between 1965-74 that makes up much of the transpiration cooling knowledge base (Kays and Moffat, 1975:223).

For instance, Simpson accomplished a study of the boundary layer on a porous wall with suction and blowing in 1968. His study showed boundary layer growth in both cases (Schetz, 1984:205), and plots from his results are shown in Figure 1.1. In contrast, Antonia and Fulachier noticed a 23% decrease in boundary layer thickness in the presence of suction

(1989:431). Scott and others made similar measurements by blowing helium through a porous plate and also saw boundary layer growth as a result (Schetz,1984:273), although it was not as pronounced as in the Simpson case (See Figure 1.2). In Figures 1.1 and 1.2, δ^* represents boundary layer displacement thickness, and actual data points are represented by the filled squares.

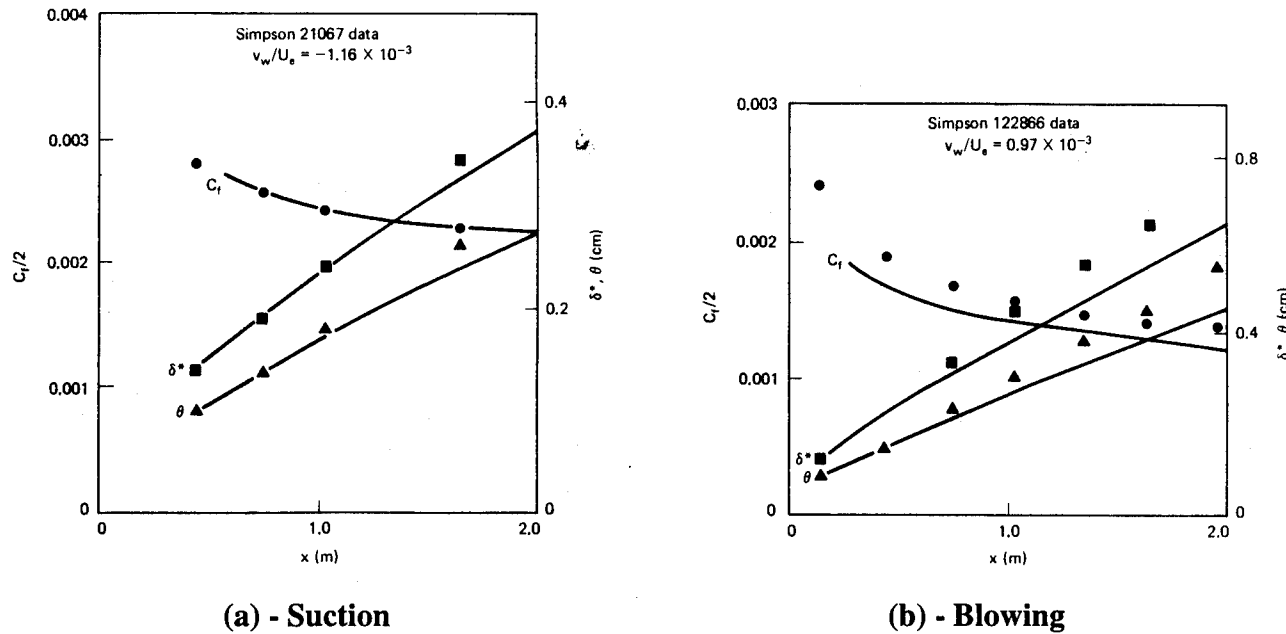


Figure 1.1 - Boundary Layer Growth w/ Blowing (Schetz,1984:205)

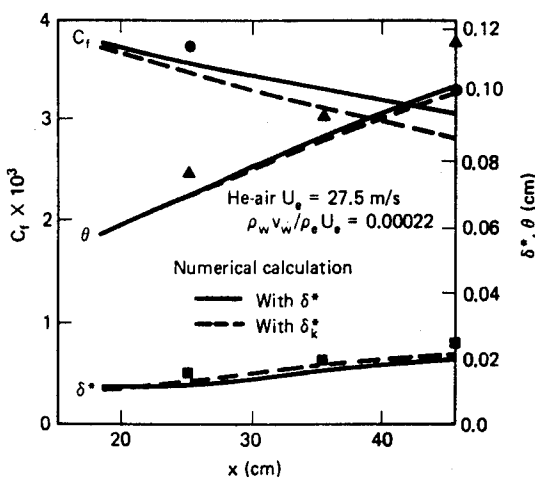


Figure 1.2 - Boundary Layer Thickness w/ Helium Injection (Schetz,1984:276)

The lines accompanying the data in Figures 1.1 and 1.2 represent the results of numerical methods developed by Schetz and Favin for predicting the boundary layer thickness with injection or suction (Schetz,1984:202,273). Their analysis used the Reichardt eddy viscosity model extended to injection and applied it to the above cases for their predictions (Schetz,1984:202). Schetz and Favin's method predicted very accurately the experimental data collected in Simpson's suction case (Schetz,1984:205) and Scott's blowing case (Schetz,1984:276), but its predictions were slightly low in the Simpson blowing case (Schetz,1984:205).

The contrasting results of Simpson versus Antonia and Fulachier and the varying results of Schetz and Favin's prediction methods point out the complexity of a transpired turbulent boundary layer. Another result from Schetz (White,1991:435) states that a porous wall actually increases skin friction (related to C_f) along a nozzle wall which would decrease the boundary layer thickness. This also means that a certain amount of blowing would be required to counteract the increase in C_f due to the porous plate before any cooling can be achieved (White,1991:436). In addition to these effects, roughness of a porous surface can also affect boundary layer growth. Therefore, the conflicting results above are not disturbing because the interrelationships between suction, blowing, and roughness are not well understood. Figures 1.1 and 1.2 only show that it is very difficult to predict the exact effect transpiration cooling will have on a given boundary layer.

An older study by Goldstein, Shavit, and Chen, involved injecting air into air through a section of porous material on a flat plate. They measured a rapid increase in boundary layer thickness at the beginning of the porous material with slower increases further downstream (Figure 1.3). Also, the thickness reached a definite maximum at a point downstream of the injection point, and far downstream the boundary layer resumed the normal shape of a boundary

layer on a flat plate (Goldstein, Shavit, and Chen, 1965:355). The results of the Goldstein et. al. study provided an indication of what to expect in this experiment as a similar situation existed. The introduction of a pressure gradient in this research did change the situation, and the results seen here were quite different.

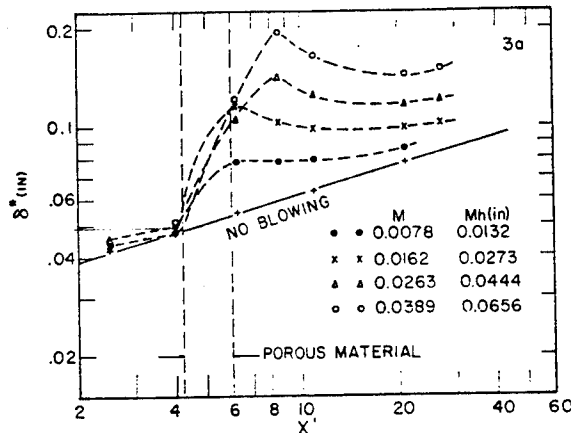


Figure 1.3 - Flat Plate Boundary Layer Growth w/ Injection (Goldstein et.al.,1965:356)

The Goldstein et. al. study also points out that when comparing injection ratios it may be better to compare injection ratio per unit length than just plain injection ratio (Goldstein et al,1965:355). This may provide a method of relating the results of experiments using different geometries to each other.

One performance study, accomplished by Azevedo, used three rows of film cooling holes in a diverging nozzle for injection and measured the effect of blowing on the thrust efficiency of the nozzle. The parameters investigated in this study included injection angle (15° - 100°), nozzle divergence angle (1° - 10°), and blowing ratio (0.01-0.08). Because transpiration cooling is essentially the limiting case of 90° film cooling, only data for the 100° injection angle case was of

interest because it was the closest to the transpiration condition. Thrust efficiency (C_v) was referenced to the ideal thrust the nozzle would produce under isentropic conditions (Azevedo,1993:47), and results were reported in terms of ΔC_v from the non blowing to the blowing case.

Not surprisingly, Azevedo found that injection at 100° caused the greatest ΔC_v : more than -0.06 or a performance loss of 6% in terms of thrust (Azevedo,1993:48). Some of Azevedo's results are shown in Figures 1.4a and b. The largest injection angle caused the largest performance loss because larger injection angles cause greater flow disturbances, which take more energy to overcome.

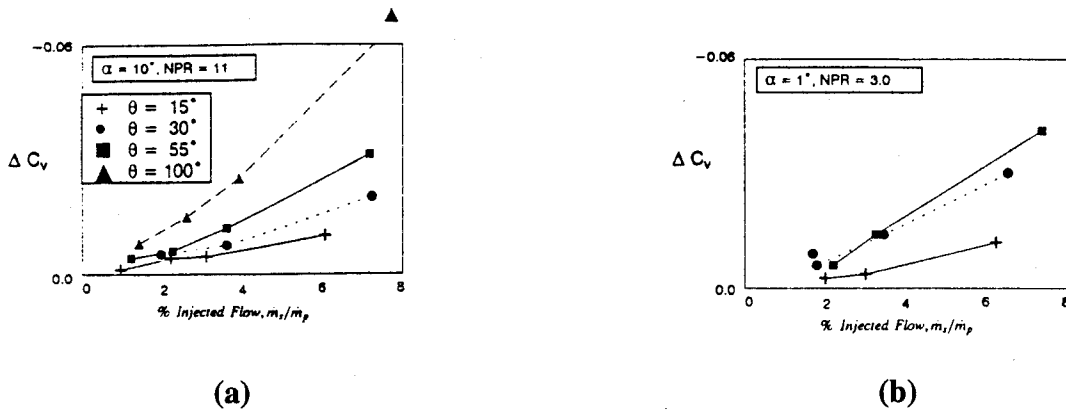


Figure 1.4 - Thrust Losses w/ Film Cooling in a Nozzle (Azevedo,1993:48)

Azevedo's study applied to this experiment because it gave an idea of the effect that injection by transpiration could have on the performance of a nozzle. However, Azevedo's results were very specific to the geometries he tested because it is very difficult to translate the results of one experiment involving a pressure gradient to another. Therefore, Azevedo's results probably had little bearing on this experiment except as an order of magnitude comparison. It was expected that results in this experiment would show smaller performance losses than were

reported by Azevedo because the injection velocities were much smaller, which caused smaller flow disturbances.

In another performance study by Aerojet, a platelet design for a porous wall was used. This type of design addressed the problem of varying blowing ratios due to varying pressure drops along the porous wall by decreasing port size with increasing pressure drop. Flow through a porous wall of uniform porosity wall always seeks the path of least resistance, which is where the greatest pressure drop occurs. In a nozzle, the pressure drop increases along the nozzle while temperature decreases. Therefore, flow through a nozzle wall of uniformly porous material is not directed to the throat, which is the hot spot. A platelet design better directs the cooling flow to hot spots in a nozzle instead of allowing flow to go to low temperature areas, which do not require as much cooling.

The Aerojet study was a combustion study that used transpiration cooling with RP-1 liquid rocket fuel as the coolant. It employed injection flow rates from 9.98-61.2 kg/s (22.0-135.0 lb_m/s) at chamber pressures from 8.2-19.3 MPa (1192-2804 psi) and compared the engine's performance to an engine using regenerative cooling. Besides reducing the heat transfer by an impressive 97%, with transpiration cooling they were able to actually increase the rocket's specific impulse by as much as 10 sec over regeneratively cooled systems (May and Burkhardt, 1991:53). Since specific impulse, or I_{sp} , is a parameter of interest in this experiment, this was an interesting result.

1.4 Objectives and Scope

In one sense, using transpiration cooling in a model with complex geometry and a pressure gradient made the scope of this experiment broad because it pushed the envelope of current knowledge. At the same time, however, the scope was necessarily small for the same reason. Extending the envelope of current knowledge opened up nearly endless permutations of combinations of porous material thickness, porosity, area, position in the nozzle, and blowing ratio. This research only hoped to scratch the surface of new possibilities with transpiration cooling and begin relating the parameters of interest to each other. Test conditions were kept as constant as possible over the many test runs conducted, and data was collected using a single nozzle geometry with a single thickness (made up of four layers of equal thickness material) and area of porous material over a range of low blowing ratios (0.0 - 0.011).

Within the above scope, the objectives of this research were to understand the differences between flow over a porous and non porous wall with no blowing, to relate blowing ratio to boundary layer thickness on a porous wall, to relate blowing ratio to the uniformity and magnitude of the exit Mach number across the exit plane of the nozzle, and relate the above results to the performance of the nozzle.

1.5 Methodology

A Mach 2.0 characteristic nozzle was designed and installed in the AFIT low pressure shock tunnel, which can produce high pressure, high temperature chamber conditions. Chamber pressure and temperature were approximately 482 kPa (70 psi) and 475 K respectively. One side of the nozzle (the non blowing side) was constructed with no modifications as a control in the

experiment, and the other (the blowing side) was modified to accommodate transpiration by replacing much of the wall with porous material.

The run times in the shock tunnel were very short (i.e., milliseconds) so high speed, precision transducers were required for data collection. A total of 11 pressure transducers were used to collect the data necessary for complete analysis of transpiration cooling effects. Transducers were placed along both walls of the supersonic portion of the nozzle, in the converging section of the nozzle, in the constant pressure blowing plenum, in a pitot probe for exit pressure measurements, and along the top of the tunnel for shock speed measurements.

Five data sets were collected during this experiment: one baseline set and four with blowing. Many runs with no blowing in the nozzle were conducted to refine testing procedures, test conditions, and completely understand the model's flow features at baseline conditions in terms of chamber conditions, wall Mach number, and exit Mach number profile. Shock speed was also determined to have a large effect on chamber conditions during this phase of the experiment. Chamber conditions, wall Mach number, and exit Mach number data were also taken with blowing for comparison with baseline data. As mentioned earlier, only low blowing ratios were considered.

Another source of data besides the transducers was shadowgraph photography accomplished during this experiment because they were the only source. Shadowgraphs were used during the baseline phase of the experiment to visualize the initial shock wave propagation through the nozzle, initial start up dynamics, established flow, and unstart dynamics. These photographs were also used to estimate the run time of the nozzle. In addition, the effects that the porous wall without blowing had on the flow field were determined from the photographs.

Boundary layer thickness measurements were taken from shadowgraphs of established flow at each blowing ratio to see the effect of transpiration on the boundary layer thickness. Finally, shadowgraphs proved useful at other times for solving data collection problems.

Transducer data for each run was reduced using computer programs written specifically for this experiment. Run times varied slightly for each run, which did cause variations in the results. The calculated average values for data presented here include a Student t 99% confidence interval.

Blowing ratio was defined throughout this experiment as:

$$B = \frac{1}{s} \int \frac{\rho_i u_i}{\rho_\infty u_\infty} ds \approx \frac{1}{s} \sum \frac{\rho_i u_i}{\rho_\infty u_\infty} \Delta s \quad (1-1)$$

where: B = blowing ratio

s = arc distance along blowing area

ρ = gas density

u = gas velocity

i = injected gas condition

∞ = freestream gas condition

This definition for blowing ratio was chosen because it removed area dependence from the calculation, and it took into account the recommendation of Goldstein et. al. (1965:355) that using a blowing ratio per unit length is better than just blowing ratio alone.

II. Theory

Before embarking on the study of transpiration effects on boundary layer thickness and performance, some boundary layer theories related to this study should be reviewed. Specifically, this study was interested in the effects of boundary layer growth in the presence of a favorable pressure gradient on the performance of a nozzle. Therefore, only theories leading to boundary layer thickness calculations are reviewed here. First, however, some facts and basic boundary layer relations should be reviewed.

2.1 Turbulent Boundary Layer

Prandtl first introduced the concept of a viscous boundary layer in 1904 and showed that a flow field could be broken into a thin viscous layer near the wall and the freestream, which is essentially nonviscous (Hill and Peterson, 1992:95). Since then, knowledge of the boundary layer has flourished, and distinctions between laminar and turbulent layers have been made as well as characterization of the transition from one type to the other. This review will concentrate on turbulent boundary layer theory because this type of boundary layer was expected in this experiment.

Engineering applications such as airfoils, inlets, and turbine blades that can have a turbulent boundary layer almost always perform better because of the superior pressure recovery that can be obtained with turbulent over laminar boundary layers. Therefore, it is generally advantageous to have a turbulent boundary layer. Turbulence is a very complex phenomenon, and completely analyzing it is a nearly impossible task (White, 1991:394). There is currently no purely analytical treatment of turbulence, and therefore, understanding it depends on experimental

observation (Hill and Peterson, 1992:111). Equations have been developed semiempirically to deal with turbulent boundary layer analysis, but as more data was collected, the basic boundary layer equations were extended. These extensions provided tools for dealing with turbulent boundary layers in a variety of situations including the transpired boundary, which was of interest here.

The equations given in the following development assume a steady, two-dimensional, incompressible boundary layer. Also, this development can be found in a more complete form in Hill and Peterson (1992:102-105). The development begins, as always, with a control volume (Fig 2.1) and the continuity and momentum equations, Eq.2-1. Velocities in the x and y direction are represented by u and v respectively.

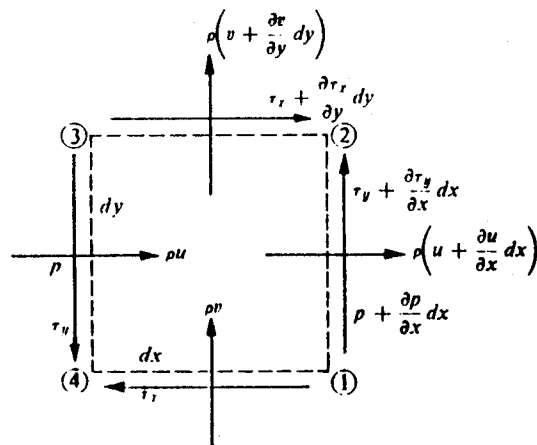


Figure 2.1 - Control Volume

$$\frac{\partial u}{\partial x} + \frac{\partial v}{\partial y} = 0 \quad (2-1a)$$

$$u \frac{\partial u}{\partial x} + v \frac{\partial u}{\partial y} = -\frac{1}{\rho} \frac{dp}{dx} + v \frac{\partial^2 u}{\partial y^2} \quad (2-1b)$$

Integrating the momentum across the boundary layer is a useful approximation for solving the boundary layer equations, and Eq.2-2 shows the general form of the momentum integral equation after algebraic manipulation from its original form in Eq.2-1b

$$\int_0^h \frac{\partial}{\partial x} [u(U-u)] dy + \frac{dU}{dx} \int_0^h (U-u) dy = + \frac{\tau_0}{\rho} \quad (2-2)$$

where: h = an indefinitely large quantity

τ_0 = wall shear stress

ρ = flow density

u = velocity of flow inside the boundary layer

U = freestream velocity

The quantity $(U - u)$ is called the mass flow defect, which is a result of the decreased flow velocity in the boundary layer due to friction. In this region of the boundary layer, the mass flow rate is actually less than the freestream flow. For a nozzle to enclose only uniform velocity freestream flow, the boundary layer would have to remain in place, and the walls bounding the flow would have to be displaced inward. The flow region excluded by moving the walls inward is called the displacement thickness (δ^*) because this region is unavailable to the freestream. Displacement thickness is defined by Equation 2-3a. The quantity $u(U - u)$ is similarly defined as the momentum defect, and has an associated thickness (θ) defined by Eq.2-3b. The upper limits of integration can be infinity in Eq. 2-3 because outside the boundary layer $u = U$, and the integral goes to zero.

$$\delta^* = \int_0^\infty \left(1 - \frac{u}{U}\right) dy \quad (2-3a)$$

$$\theta = \int_0^{\delta^*} \frac{u}{U} \left(1 - \frac{u}{U}\right) dy \quad (2-3b)$$

where: δ^* = displacement thickness

θ = momentum thickness

Plugging these definitions into Eq.2-2 gives the most commonly used forms of the momentum integral equation, Eq.2-4. This equation applies to both laminar and turbulent boundary layers, but requires knowledge of the relationship between δ^* and θ to solve. This knowledge can be gained with use of a shape function (not considered here) or by numerical momentum integral methods.

$$\frac{d}{dx} (U^2 \theta) + \frac{dU}{dx} (U \delta^*) = \frac{\tau_0}{\rho} \quad (2-4)$$

or

$$\frac{d\theta}{dx} + (2 + H) \frac{\theta}{U_e} \frac{dU}{dx} = \frac{C_f}{2}$$

where: $H = \theta / \delta^*$

U = freestream velocity

C_f = coefficient of friction

The general boundary layer equations developed above have been extended and applied to turbulent boundary layers with a pressure gradient. Solutions to the equations for this case can also be solved by at least two numerical momentum integral methods, which are discussed here.

First, a formulation by Moses estimates the boundary layer growth in nearly two-dimensional flow with pressure gradients. The following development of Moses's relationships can be found in Hill and Peterson (1992:119-121). Moses's method begins with minor changes to the momentum integral equation (Eq.2-2).

$$\int_0^y \frac{\partial}{\partial x} [u(U-u)] dy + \frac{dU}{dx} \int_0^y (U-u) dy = + \frac{\tau_0}{\rho} - \frac{\tau_1}{\rho} \quad (2-5)$$

where: y_I = any location within the boundary layer

τ_I = local shear stress at $y = y_I$

To solve Eq 2-5, the quantities δ^* and θ must be known, and δ^* can be found using Eq.2-3a where the upper limit of integration is the actual boundary layer thickness, δ . Solving for θ is not straight forward because local wall shear stress can not be related to local pressure gradient in turbulent flow (Hill and Peterson, 1992:119). Instead, Moses integrated Eq.2-5 from $y = 0$ to $y = 0.3\delta$ making use of the velocity profiles in two regions of the boundary layer: the nearly laminar inner layer and the turbulent outer layer.

A velocity profile determined by Moses for each region was used to define a momentum integral containing terms related to the skin friction, local Reynolds number, freestream velocity, and kinematic viscosity. Each term in the equations had a different coefficient assigned to it for a total of eight coefficients. These coefficients are functions that have to be calculated separately during an iteration. If a full numerical integration is not desired, δ^* and θ can be approximated at discrete points along a nozzle wall, where the boundary layer thickness is known, with Eqs. 2-6 and 2-7.

$$\frac{\theta}{\delta} = \alpha - 0.5\beta - 2\alpha^2 + 1.58333\alpha\beta - 0.37143\beta^2 + (-49.5 + 300\alpha)/\text{Re}_\delta \quad (2-6)$$

$$\frac{\delta^*}{\delta} = \alpha - 0.5\beta + 49.5/\text{Re}_\delta \quad (2-7)$$

where: $\alpha = \frac{1}{0.41} \sqrt{\frac{C_f}{2}}$

$$\beta = \alpha [\ln(\alpha \text{Re}_\delta) + 1.1584] - 1$$

$$C_f = \frac{\tau_0}{\frac{1}{2} \rho U^2}$$

$$\text{Re}_\delta = \frac{U\delta}{\nu}$$

$$\tau_0 = \frac{\Delta p R}{2L}$$

and: τ_0 = local wall shear stress

Δp = pressure drop in length L

R = radius of channel

ν = local viscosity

δ = boundary layer thickness

The boundary layer is often separated into three regions when considering boundary layer velocity profiles. There is an inner layer where viscous shear dominates, an outer layer where turbulent shear dominates, and an overlap layer where a smooth transition between the inner and outer layer occurs (White, 1991:411). The velocity profile in a turbulent boundary layer varies depending on the type of pressure gradient present, but the log-law using inner layer variables is

used to relate any type of pressure gradient to a single velocity profile. The log-law with inner variables is given in Eq.2-8.

$$\frac{u}{v^*} = \frac{1}{\kappa} \ln \frac{yv^*}{v} + B \quad (2-8)$$

where: $v^* = \left(\frac{\tau_w}{\rho} \right)^{1/2}$

and: v = local viscosity

τ = wall shear stress

y = distance from wall

u = flow velocity inside boundary layer

$\kappa = 0.41$

$B = 5.0$

Coles made the log law better by noticing that excess velocity in the outer layer, which the log-law only adequately predicts, has a wavelike shape (White,1991:417). Therefore, a wake function was added to the log-law, which makes its velocity profile predictions more accurate. Defining $u^+ = u/v^*$ and $y^+ = yv^*/v$, the log-law with the addition of Cole's Law of the Wake is given in Eq.2-9.

$$u^+ = \frac{1}{\kappa} \ln(y^+) + B + \frac{2\Pi}{\kappa} f\left(\frac{y}{\delta}\right) \quad (2-9)$$

where: $\Pi = \frac{\kappa A}{2}$

and: A = outer-variable constant (1.0 for a strong favorable pressure gradient)

B = inner-variable constant (5.0)

Π = Cole's wake parameter

Equation 2-9 is complete and accurate for any two-dimensional, turbulent boundary layer profile, and if it is integrated over the boundary layer, δ^* and θ can be determined from Eq.2-10. Notice that in this case the skin-friction coefficient is related to Π and λ . This makes the calculation of C_f much simpler and could be applied in this form to other analyses.

$$\frac{\delta^*}{\delta} = \frac{1 + \Pi}{\kappa \lambda} \quad (2-10a)$$

$$\frac{\theta}{\delta} \approx \frac{\delta^*}{\delta} - \frac{2 + 3.2\Pi + 1.5\Pi^2}{\kappa^2 \lambda^2} \quad (2-10b)$$

where: $\lambda = \left(\frac{2}{C_f} \right)^{\frac{1}{2}}$

$$\left(\frac{2}{C_f} \right) = \frac{1}{\kappa} \ln \left(\frac{Re_\delta}{\lambda} \right) + B + \frac{2\Pi}{\kappa}$$

By combining the two methods developed above, an approximate analysis of the boundary layer thickness at the exit can be accomplished, but this is accurate for a non blowing wall only. The boundary layer would be thicker on a blowing wall because of the rough porous plate.

Assuming that the porous plate is fully rough and $\frac{k}{x} = \frac{Re_x}{1000}$, C_f and Re_x can be corrected for roughness with Eqs. 2-11 and 2-12 and the above analysis reaccomplished.

$$Re_x \approx 1.73(1 + 0.3k^+) e^Z \left[Z^2 - 4Z + 6 - \frac{0.3k^+}{1 + 0.3k^+} (Z - 1) \right] \quad (2-11)$$

$$C_f \approx \left[2.87 + 1.58 \log_{10} \left(\frac{x}{k} \right) \right]^{-2.5} \quad (2-12)$$

$$Z = \kappa \lambda$$

$$\text{where: } k^+ = \frac{\text{Re}_x(k/x)}{\lambda}$$

and: k = roughness height

Another useful analysis is estimating the boundary layer thickness at the throat of a nozzle because the thickness is often too small to measure visually. The discharge coefficient is a well known quantity in rocket nozzle, and is given in Eq. 2-13 where R is defined by Eq 2-14.

$$C_D = 1 - \left(\frac{\gamma + 1}{2} \right)^{\frac{1}{4}} \left\{ \frac{-2.128}{\gamma + 1} + 3.266 \right\} R^{-\frac{1}{2}} + 0.9428 \frac{(\gamma - 1)(\gamma + 2)}{(\gamma + 1)^{\frac{1}{2}}} R^{-1} \quad (2-13)$$

$$R = \text{Re}^* \left(\frac{R^*}{R_c} \right)^{\frac{1}{2}} \quad (2-14)$$

where: γ = ratio of specific heats (c_p/c_v)

Re^* = Reynolds number at the throat

R^* = throat radius

R_c = radius of curvature of the throat

It can be shown that for cases where $\delta_t / R^* \ll 1$, the boundary layer thickness at the throat can be estimated by Eq.2-15. Using this method for the nozzle used in this experiment, δ_t was estimated to be 0.018 mm (0.0007") (See Appendix E). In this study, boundary layer thickness was assumed to be 0.018 mm when the boundary layer thickness was not visually measurable.

$$\frac{\delta_t}{R^*} = \frac{1 - C_D}{2} \quad (2-15)$$

2.2 Transpired Turbulent Boundary Layer

One approach to the transpired boundary layer was presented by Kays and Crawford (1980:180-181). They developed an algebraic Couette flow solution assuming flat plate conditions. They found that the skin friction at a given blowing ratio can be successfully approximated Eq. 2-16, where the blowing ratio is defined in Eq. 2-17.

$$\frac{C_f/2}{(C_f/2)_0} = \frac{\ln(1 + B_f)}{B_f} \quad (2-16)$$

$$B_f = \frac{\dot{m}''/\dot{m}_\infty}{C_f/2} \quad (2-17)$$

where: \dot{m}'' = mass flow rate through the porous wall

\dot{m}_∞ = freestream mass flow rate

Equations 2-16 and 2-17 are solved simultaneously to calculate the change in $C_f/2$ with blowing. Once the new $C_f/2$ is known, roughness can be taken into account, and other methods to approximate the boundary layer thickness with transpiration can be used.

Another approach to determining the effect of transpiration on the boundary layer is to modify the log-law with another logarithmic term, which was accomplished by Stevenson (White, 1991:435). His modified log-law, defining $v_w^+ = v_w / v^*$, is given in Eq. 2-18. With this

equation, law of the wall plots can be created that include blowing and allow an estimate of C_f reduction with blowing to be obtained. After correcting C_f , the boundary layer thickness with blowing can be approximated using the previous analyses by Moses and Coles.

$$\frac{2}{\nu_w^+} \left[(1 + \nu_w^+ u^+)^{1/2} - 1 \right] \approx \frac{1}{\kappa} \ln(y^+) + B \quad (2-18)$$

It should be noted that porous plates cause roughness and disturbance effects on the boundary layer, but it was assumed that roughness caused the same effect in each case, and any additional growth beyond that was a result of blowing.

III. Experimental Setup

3.1 Shock Tunnel Configuration

According to shock wave theory, when a shock wave passes through an undisturbed fluid it increases the pressure and temperature of the fluid behind it (Shapiro, 1954:116) as well as accelerating the fluid in the direction of the shock wave (Shapiro, 1954:998). If the shock wave reflects with equal strength from a straight wall the same effect occurs but the acceleration is in the opposite direction causing the fluid's net velocity to be zero behind the shock with even higher pressure and temperature. This is the reason shock tunnel facilities are suited for this kind of experiment (Shapiro, 1954:1021,1008). The "pocket" of zero velocity, high pressure, high temperature air resulting from the reflected shock provided the simulated chamber conditions for the present study.

The AFIT low pressure shock tunnel was the facility used for this experiment, and Figure 3.1 shows a schematic of the facility including all external connections. The shock tunnel has a 1.22 m (4') driver section, a 4.88m (16') driven section, a 1.22 m (4') test section, and is 20.3 cm (8") tall by 10.2 cm (4") wide. This experiment used a 0.18mm (0.007") mylar diaphragm to separate the high pressure section from the low pressure section.

The tunnel was operated with an air/helium driver mixture, which increased the strength of the shock and the chamber conditions to a level higher than an air only driver would have produced (Shapiro, 1954:918). Using an air/He driver mixture changes the ratio of specific heats (γ) in the driver, and this value must be known to accurately calculate the chamber conditions after shock reflection. Appendix A shows an example calculation of γ for the air/He mixture.

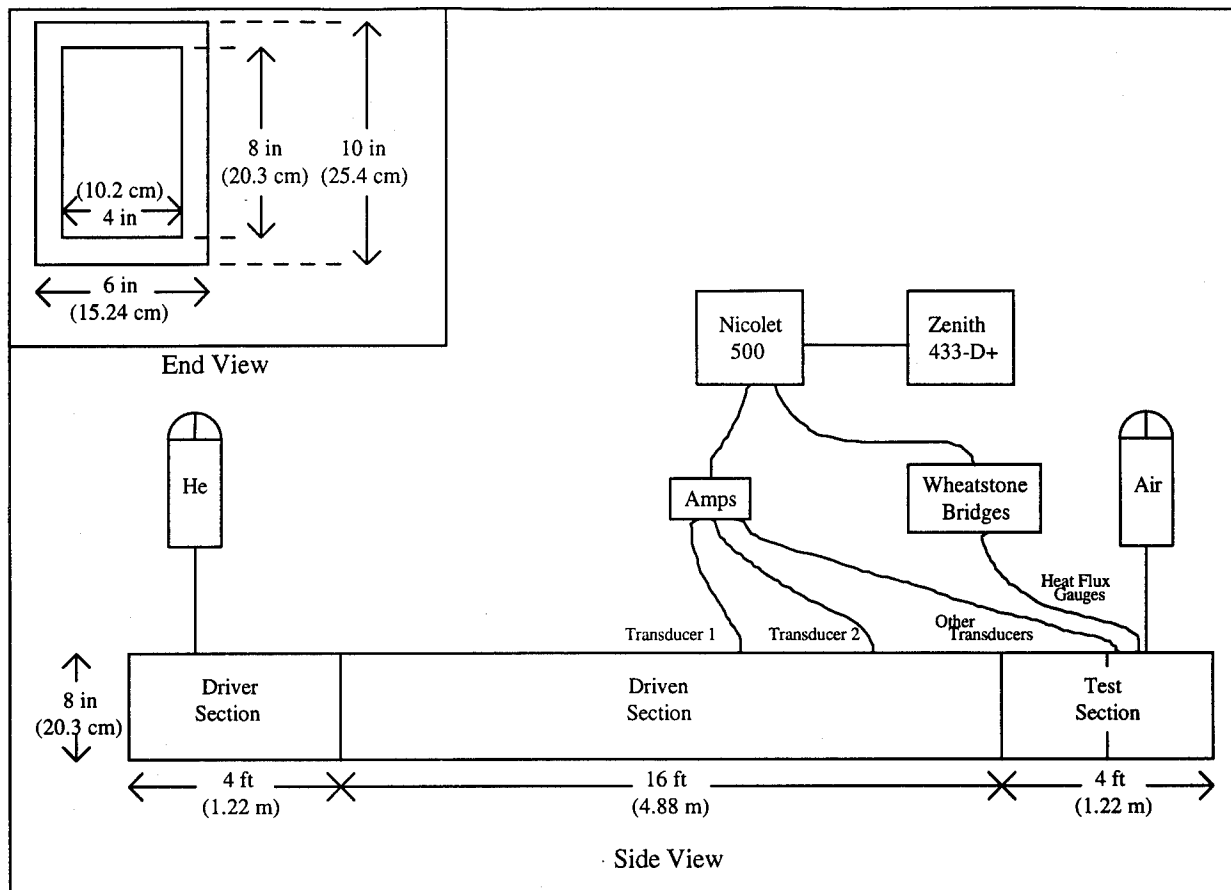


Figure 3.1 - Shock Tunnel Configuration

In this experiment, simulated chamber conditions were produced when the shock wave reflected from the converging section of a Mach 2.0 characteristic nozzle located in the test section so that the driven section was 5.49 m (18') long. Knowing the driven section length, pressure and temperature as well as the driver pressure, temperature, and γ , the chamber conditions could be predicted according to shock tunnel theory (Shapiro, 1954:1008-1009). Program SHOCKTUN.FOR (Bowersox, 1990) calculated the conditions in each region of the shock tunnel for given test conditions, and although test conditions varied slightly from run to run, Table 3.1 shows the design driver conditions, analytical chamber conditions, and analytical

run time for the experiment. Appendix B contains instructions for using SHOCKTUN.FOR. It was expected that the actual chamber conditions would be less than the values shown in Table 3.1 because the shock wave was not perfectly reflected from the converging walls of nozzle and some of the shock wave was swallowed by the nozzle.

Table 3.1 - Summary of Expected Test Conditions

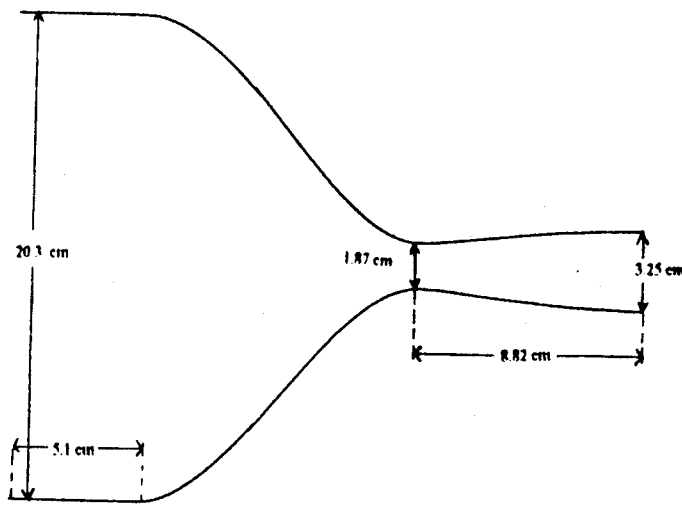
	Condition
Driver Pressure	0.58 MPa (84.4 psi)
Air	0.10 MPa (14.3 psi)
Helium	0.48 MPa (70 psi)
Driven Pressure	0.10 MPa (14.3 psi)
P5	0.71 MPa (103.1 psi)
T5	546.0 K
Run Time	8.28 ms

The only other configuration note on the shock tunnel is that the downstream end of the tunnel was left open to prevent undesirable reflections. Therefore, shock waves were allowed to pass out of the shock tunnel and into the room. This was acceptable because the exit pressure of the nozzle was close enough to atmospheric pressure that flow separation due to overexpansion and shock waves in the nozzle due to a deficient pressure ratio were avoided.

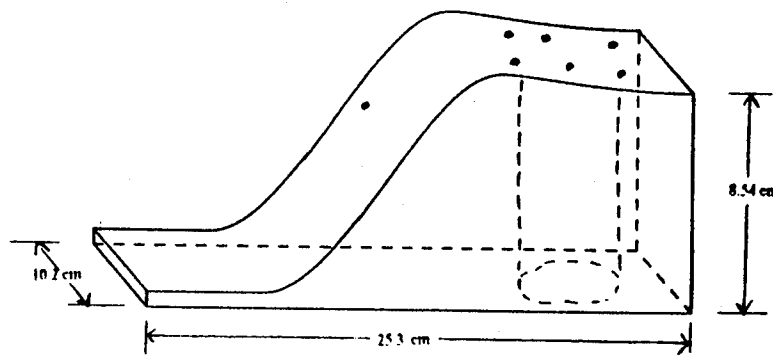
3.2 Test article

3.2.1 General Description

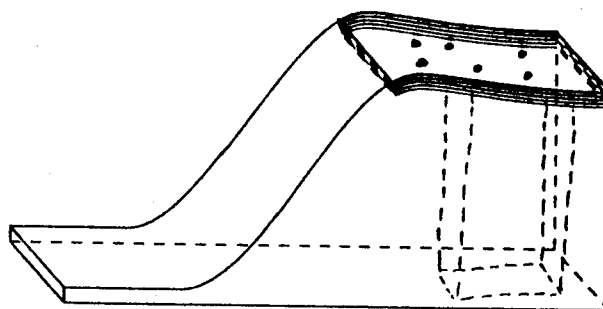
The test article used for this experiment was a Mach 2.0 characteristic nozzle designed using three computer programs written for nozzle design by Dr. Rodney Bowersox (1990). Figure 3.2 shows the features and dimensions of the model.



(a) Silhouette View



(b) Non Blowing Side View



(c) Blowing Side View

Figure 3.2 - Nozzle Design w/ Dimensions

Some nozzle features were chosen arbitrarily because the model only needed to be a supersonic nozzle appropriate for a shock tunnel study of boundary layer thickness and heat transfer reduction in a transpiration cooled nozzle. Mach 2.0 was chosen because it would clearly be supersonic even with losses included, the pressure ratio for choked flow could be achieved without drawing a vacuum in the shock tunnel, and a diffuser was not necessary to avoid flow separation and shock waves in the nozzle.

The throat size was chosen based on the requirement that it be small compared to the size of the shock tunnel so that the converging section of the nozzle would approximate a straight wall for the shock wave to reflect from. Zuppan suggested in his work that a throat/shock tunnel height ratio of 10.65 to 13.3 was appropriate for good shock wave reflection, and in his work he used a throat height of 1.91 cm (0.75") (Zuppan, 1965:Preface). Because the same shock tunnel was being used for this experiment, Zuppan's choice seemed appropriate and was adopted here. In addition, the model was designed to be as wide as the shock tunnel (4"), which made the flow two-dimensional.

One side of the nozzle was designed for transpiration cooling while the other remained impermeable to act as a control in the experiment. Instruments were inserted along the non blowing side of the nozzle through a circular cavity drilled into it from the bottom (see Fig 3.2b). Also, chamber pressure was measured from the non blowing side and a deep channel had to be drilled to insert this transducer.

The cavity on the blowing side was square and went all the way through the wall. During blowing this cavity acted as a constant pressure plenum to ensure that the porous material experienced the same pressure throughout the test as well as providing space to insert instruments

along the wall. From a point 1.27 cm (0.5") before the throat to the nozzle exit, the wall was recessed by 0.635 cm (0.25") creating a contoured shelf on the blowing side, and the four layers of the selected porous material (see Appendix F) were installed. Each layer of porous material was also shaped to the nozzle contour individually to minimize the unevenness at the porous material/aluminum seam, which could trip the flow and disrupt the flow field downstream (see Figure 3.2c). Even with this precaution there was still enough unevenness at that point to trip the flow (see Figure 3.3). Because the flow tripped in the converging section where the flow was subsonic, it quickly reattached to the wall.

The selected porous material was 1.57 mm (0.062") thick 316L sintered stainless steel with 2 micron porosity, which was selected based on strength, mass flow rate, and pressure drop considerations. The porous surface was clearly more rough than the non blowing side, and the boundary layer was expected to be thicker on the blowing side in all cases.

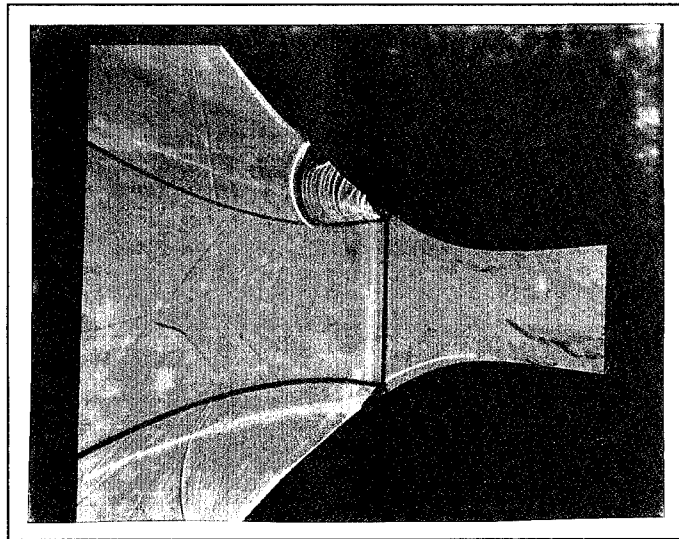


Figure 3.3 - Tripped Flow at Porous Material/Aluminum Seam

3.2.2 Nozzle Design Tools

As mentioned, three computer programs were used to design the Mach 2.0 nozzle, and the mechanics of each program used will be treated briefly. Other specifics such as input and output information on each program can be found in Appendix B.

Program NOZ2.FOR (Bowersox,1990) constructed the contoured and minimum length diverging section of the Mach 2.0 nozzle shape using the method of characteristics with two characteristic reflections. Program BLCORR.FOR (Bowersox,1990) calculated the analytical boundary layer thickness at the nozzle exit and adjusted the entire diverging section contour to compensate while maintaining the desired Mach number. These adjustments change the throat and exit geometries slightly resulting in a nozzle that was not ideal according to the isentropic flow tables in Shapiro but was very close. Figure 3.2 shows the nozzle after adjustments made by this program, and the actual design had $A/A^* = 1.738$ and $M_e = 2.03$.

Program WALL.FOR (Bowersox,1990) constructed the converging section of the nozzle and attached it to the diverging section. This program was used to design the converging section of the nozzle in such a way as to enhance the shock reflection (i.e., steep walls), yet maintain a reasonable convergence rate. There is a parameter in the program that defines the length of the sloped part of the converging section, and it was chosen to be small to produce steep converging walls.

3.3 Instrumentation and Data Collection

Ambient pressure was measured with a lab barometer, and thermocouples were used to measure ambient and plenum temperatures. Other pressure measurements were collected using

10 Endevco Model 8530A-100 transducers (range: 0-100 psia) and one Endevco Model 8514A-50 transducer (range: 0-50 psia). Their signals were amplified using Endevco Model 4423 Signal Conditioners, and transducer calibration was accomplished using a standard calibration setup. Calibration data is included in Appendix C. Two Model 8530 transducers were plugged into the top of the shock tunnel itself for shadowgraph timing purposes (henceforth referred to tube transducer 1, which is further upstream of the nozzle, and tube transducer 2). The time between the pressure jumps caused by the shock wave passing by the transducers was the reference time for triggering the light source (see Section 3.4). One Model 8530 transducer was placed in the converging section of the model to measure chamber pressure, one was placed in the plenum to measure the pressure of injected air, and the other six Model 8530s transducers were placed along the nozzle in pairs directly opposite each other to measure static pressure along the wall. The Model 8514 transducer was mounted inside of a pitot probe and used to measure exit pressure. All Signal Conditioners were set to a gain of 20X except those amplifying the two tube transducer signals, which were set to a gain of 50X. Figures 3.2b and 3.2c summarize the transducer placement along the nozzle.

The Nicolet 500 Data Collection system is a commercial data collection system that operates in the Windows environment. The equipment and documentation was located in the lab area. Pressure data taken with the Nicolet was sampled at 500 kHz

3.4 Shadowgraph Flow Visualization System

A shadowgraph is a photograph, which can be taken for flow visualization. A shadowgraph system requires three basic items: an aperture, a light source, and a mirror. In

general, the mirror is placed so that light reflected from it will illuminate the area to be photographed. The light source, the mirror, and the desired image should be at the same height to ensure that the light passes perpendicularly through the flow. The light source is placed at the mirror's focal length from the mirror so that when the light is reflected from the mirror it will be a uniform column. A shallow angle between the light source and reflected column helps to ensure that the column of light is uniform. The column passes through the flow being photographed and exposes the film, and because of density gradients in the flow field, features such as shock waves and boundary layers are visible. Figure 3.4 shows the basic setup used in this experiment.

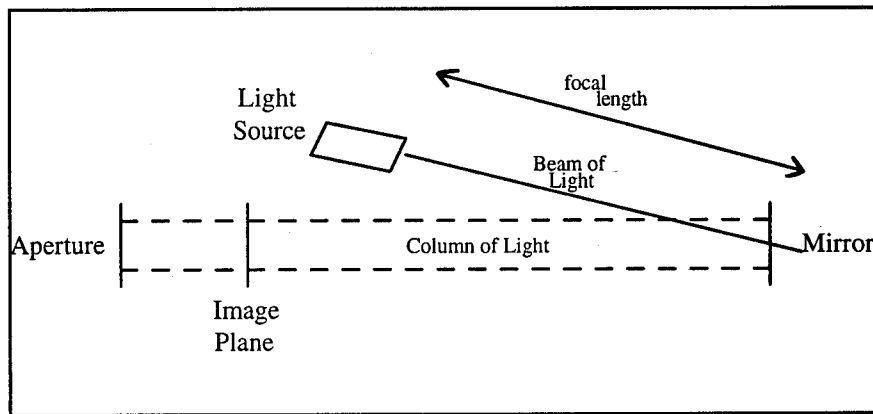


Figure 3.4 - Shadowgraph Setup

For tests with long run times, this system can be set up and the film exposed by hand at any point during the test. Run times in a shock tunnel, however, are on the order of milliseconds, and it is impossible to trigger the light source by hand during this time especially when shadowgraphs at specific points during the run time are desired. Therefore, an electrical system was employed to trigger the light source at a preset time measured in microseconds after the

shock wave passed tube transducer 2. The shadowgraph system complete with a timing circuit was setup to capture events in the nozzle before, during, and after its run time, and the system was demonstrated to be very reliable and accurate during this experiment.

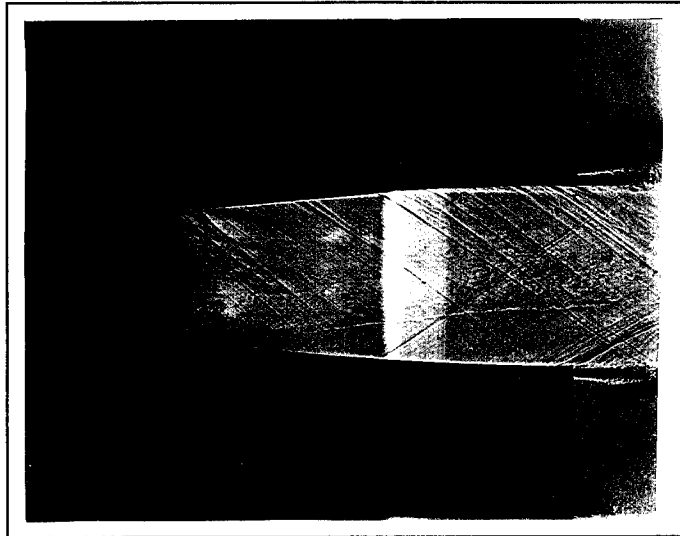


Figure 3.5 - Pitot Probe Bent Out of Flow

For example, at one point the pitot probe was not collecting usable data when it should have been. A shadowgraph was used to capture the pitot probe bent out of the flow (see Fig. 3.5) and hence, reading only ambient pressure. This discovery resulted in stiffening modifications to the pitot probe that made all pitot measurements more reliable as well as saving a lot of time and frustration in determining the source of the poor data. Table 3.2 summarizes the electrical components of the system and their functions, and Figure 3.6 shows the system in block diagram form.

Table 3.2 - Timing Circuit Components w/ function

Component	Purpose
Cordin Model 436 Proportional Delay Generator	Measure time between transducers in top of shock tunnel and output 30V pulse delayed by that time to Model 453
Cordin Model 453 Delay Generator	Output 100V pulse delayed by time on box to homemade gray box
Divider Circuit	Reduce 100V pulse from Model 453 to 5V pulse into homemade gray box
Homemade Gray Box	Output -250V pulse to trigger light source
Cordin Model 5401 Spark Lamp	Light Source
Cordin Model 5205 Power Source	Power source for spark lamp

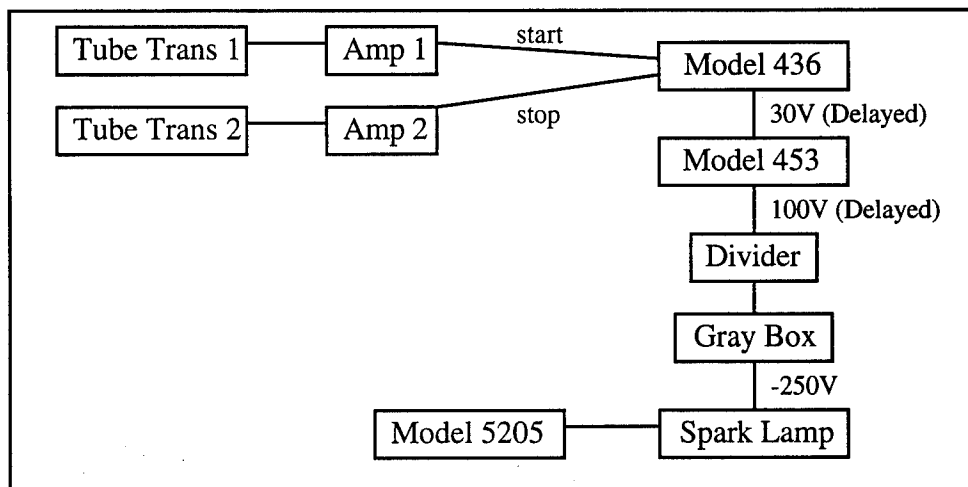


Figure 3.6 - Timing Circuit Block Diagram

The spark lamp trigger time delay began when the shock wave passed by tube transducer 2, and the total time delay is based on the measured amount of time (measured by the Model 436) between tunnel transducers 1 and 2. From Figure 3.6, then, it can be seen that the total delay period until the light source is triggered can be set to any time by satisfying Eq. 3-1.

$$TD_t = TD_{436} + TD_{453} \quad (3-1)$$

where: TD_t = total time delay (μ s)

TD_{436} = measured time delay on Model 436 (μ s)

TD_{453} = time delay set on Model 453 (μ s)

In practice, TD_{436} was measured, and TD_t was the target total time delay based on TD_{436} and the event to be captured. Therefore, the value really solved for in Eq.3-1 was TD_{453} . Using this system required at least one run at the desired test condition without a photograph but with the system running otherwise to measure TD_{436} . It was known that the distance between the two tube transducers was 0.71 m (28"), and therefore, once TD_{436} was known and assuming the shock wave propagation speed was constant, Td_t could be determined by Eq.3-2.

$$\frac{TD_{436}}{28} = \frac{TD_t}{(28+x)} \quad (3-2)$$

where: x = distance past the second tunnel transducer (in)

The proportional relationship of Eq.3-2 was used by adjusting TD_{453} appropriately and was probably most useful as a tool for capturing an initial event. In this case, x was chosen to be some point along the model. The assumption that the shock wave was moving at a constant speed held up for test runs with an air only driver as shock waves were captured at various locations along the nozzle with great accuracy. The linear relationship did not hold up for the air/He driver, which indicated that the shock wave had actually slowed down slightly after passing by the tube transducers. A correction of 250 μ s was added to TD_{453} to capture the initial event.

Once one event was captured, TD_{453} was simply incremented forward and backward until the desired range of events was captured. This range might include such highlights as nozzle start, established flow, and unstart. Test conditions changed from run to run, which affected TD_{436} , and changed the delay slightly for each run. Experience in this experiment indicated that if the conditions did not vary greatly (i.e., driver pressure within 1 in Hg) then TD_{436} varied by 10 μ s at most. Because the run times were on the order of milliseconds, this difference never caused the desired event to be missed.

The general procedure for using the timing system, then, was to run a test to measure the approximate TD_{436} , set TD_{453} to an appropriate value for capturing the desired event, run the test, and reset the system. The most important component to reset was the homemade gray box because it was a high voltage component that stored its -250V pulse in a capacitor that would quickly burn up if not reset. The box was reset by pushing the small orange button, and the orange light should come on. Shadowgraph procedures were incorporated into the shock tunnel operation procedures because the two procedures did occur simultaneously (see Appendix D for procedures).

Documentation is available on all components with the exception of the homemade gray box and divider circuit. The homemade gray box has no documentation except what is provided here, and Figure 3.7 shows a schematic of the divider circuit.

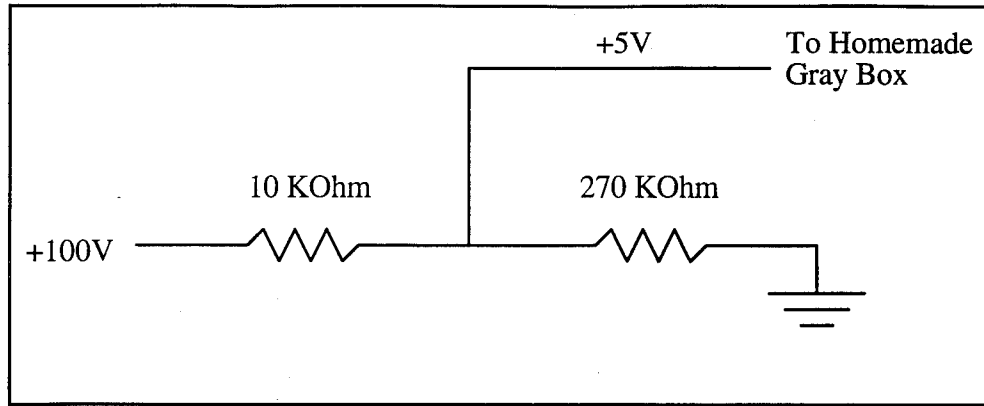


Figure 3.7 - Schematic of Voltage Divider Circuit

3.5 Procedural Notes

There are a few miscellaneous items that need to be discussed on the setup and operation of the AFIT low pressure shock tunnel. First, the driver pressure is measured in in Hg when running a test and unit conversions should be double checked for accuracy to ensure the correct test conditions are being used. Also, the diaphragm stretches as the driver is pressurized, which is expected, but this stretching can cause the shifting of the diaphragm if it is not secured tightly into place. This condition tended to cause premature bursting of the diaphragm. Periodic clicking sounds as the driver is pressurized is a warning signal for this condition.

Next, it was found that after a test using an air/He driver the entire tunnel was filled with the air/He mixture, and if a test was run immediately after the previous one this new mixture in the driven section affected the shock speed. Therefore, a five minute helium purge period was instituted between each test in which house air is forced through the tunnel to evacuate excess helium. Shock speed results were very consistent after the procedure was implemented.

Also, when taking shadowgraphs, it is important to remember that the film is exposed throughout the test so the test area must be very dark to avoid unwanted or premature exposure.

Lastly, if the shock tunnel is run with the end open as in this experiment, ear protection should be worn because it is very loud. Also, it is best if the lab door is closed, and all personnel in the room should be warned when a test is about to be run before every test.

IV. Results and Discussion

4.1 Baseline Results

4.1.1 Actual Test Conditions

Recall that it was expected that the actual chamber conditions would be less than SHOCKTUN.FOR predictions because the shock wave was reflecting from a converging nozzle section instead of a straight wall. In fact, chamber pressure and temperature were 32% and 12% less than predictions respectively. Temperature inside the shock tunnel was not actually measured, however, but was estimated with SHOCKTUN.FOR according to what the chamber pressure would have been if the measured P_0 were the actual chamber condition after a perfect reflection. Chamber temperature (T_0) was estimated at other chamber conditions using the proportional relationship,

$$T_0 = (0.86999 \left(\frac{P_0}{103.1} \right) / 0.06716) \cdot (545.978 \text{ K}),$$

which was based on the difference between predicted and actual conditions. This was acceptable because chamber pressure did not vary outside the linear range. Table 4.1 summarizes the actual test conditions for the experiment.

Table 4.1 - Summary of Actual Test Conditions

	Condition	% Error
Driver Pressure	580 kPa (84.3 psi)	---
Air	98.6 kPa (14.3 psi)	---
Helium	482.5 kPa (70 psi)	---
Driven Pressure	98.6 kPa (14.3 psi)	---
P5	482.3 kPa (69.983 psi)	$\pm 1.04\%$
T5	480.1 K	$\pm 1.04\%$
Shock Speed	527.54 m/s	$\pm 0.11\%$
Run Time	1.938 ms	$\pm 3.92\%$

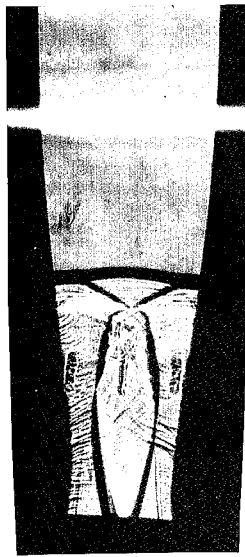
Notice from the error column of Table 4.1 that conditions were very repeatable, especially the shock strength, which was proportional to the shock speed. The shock speed was calculated based on the time it took the shock wave to pass the tunnel transducers. Test conditions were consistent enough that the data was reduced without normalization in all cases except the specific impulse analysis.

The run time in Table 4.1 was 76% lower than predicted (See Table 3.1). This was due, in part, to losses, but was mostly due to the different definitions of run time used in the two tables. In Table 3.1, run time was defined as the time between shock wave reflection and the contact discontinuity reaching the end wall. In Table 4.1, the run time was defined as the time after shock wave reflection that the nozzle maintained steady state flow conditions. The end of the run time, then, was defined as the time when the nozzle pressure ratio became deficient because of chamber pressure depletion and unstart occurred.

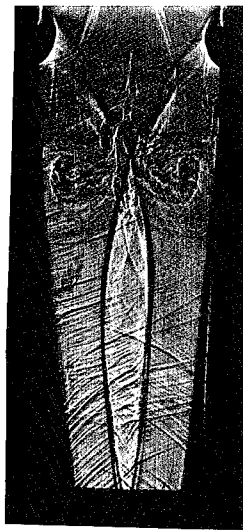
Shadowgraphs were vital to bracketing the actual run time of the nozzle because they showed very clearly the start and unstart of the nozzle. Because the timing of each photograph was known (i.e., the timing circuit, Sec 3.4), the run time could be estimated. Run times were measured accurately from pitot probe data that also showed clearly the beginning and end of steady state flow (See Figure 4.1f).

4.1.2 Characterization of the Flow Field

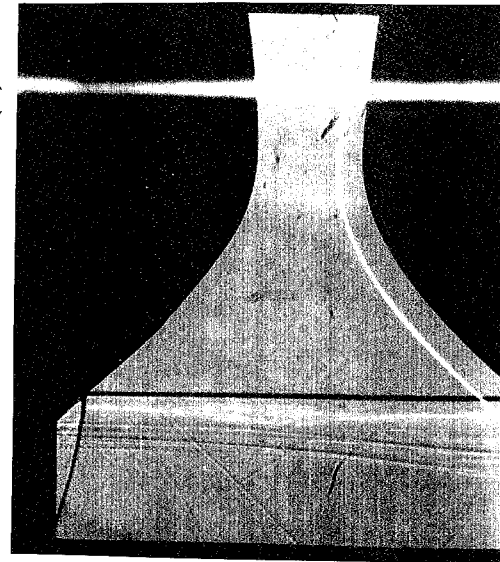
Shadowgraphs were taken at several times during the nozzle starting process to visualize and understand the events leading to established flow in the nozzle. The photographs did point out that the flow established at each point along the nozzle about 1 ms after the shock wave



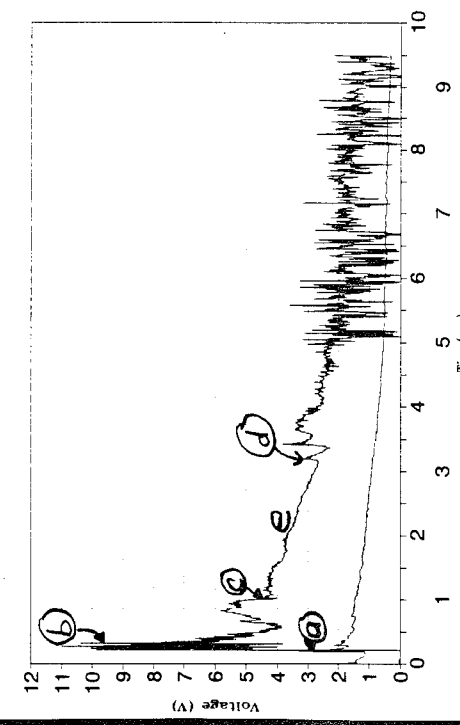
(b) Swallowed Shock



(c) Shock exiting nozzle



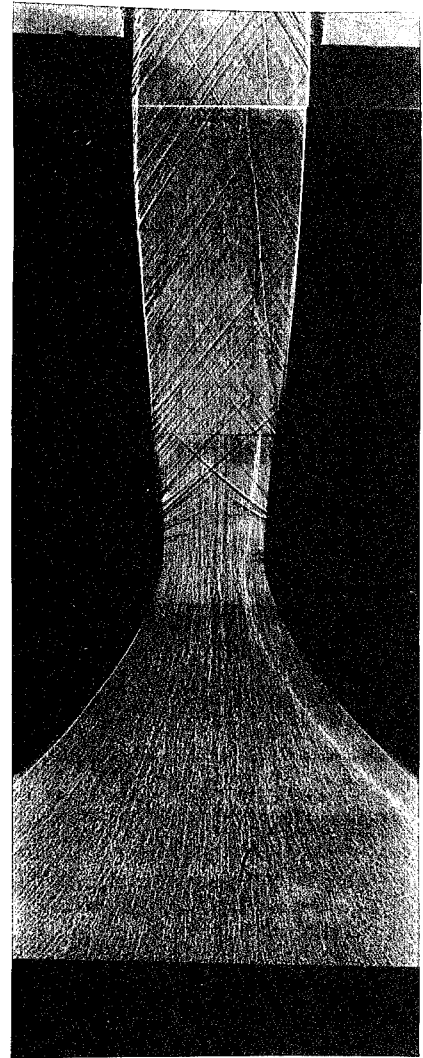
(a) Initial Shock Reflection



(f) Typical Pressure Traces



(d) Unstart



(e) Established Flow, Entire Nozzle

Figure 4.1 - Characterization of Flow Dynamics

passed by, and this was a data landmark. Figure 4.1 is a pictorial summary of a non blowing test run from initial shock wave reflection to unstart, which took place in about 3.5 ms.

In the photos, the flow is propagating from left to right, and the upper wall is the blowing side of the nozzle. This photograph orientation is maintained throughout this report. The pressure traces shown are centerline pitot probe and chamber pressure, and they are representative of runs throughout the experiment (See Figure 4.1f). Constant chamber pressure over all test runs was attributed to test condition consistency. All pitot traces showed the same general form except that run times were shorter when the probe was close to the wall because of the unstart geometry (See Figure 4.1e). These shadowgraphs are also typical because blowing had no visible effect on the start up dynamics. Figure 4.1 also helps to characterize the difference between the non blowing side and the blowing side under baseline conditions.

4.1.3 Non Blowing vs Blowing Side

Figure 4.1c shows the entire nozzle at steady state conditions including boundary layer establishment and growth along the nozzle. In the photo, the thin, bright region near each wall is the boundary layer for that side of the nozzle, and there is clearly a visible difference in thickness between the two sides. Using a caliper micrometer, boundary layer thickness measurements were made from the actual photographs and from projected images of the photographs. Several trial measurements were taken, and the statistical average of those measurements for each case was defined as the boundary layer thickness. Measurements were made the same way at positions along the nozzle to show the rate of boundary layer growth. The exit boundary layer thickness

was of the most interest because this thickness decreased the effective exit area of the nozzle, which affected its performance.

For the baseline case, the exit boundary layer thickness was 213% greater on the blowing side than on the non blowing side. Table 4.2 compares the exit boundary layer thicknesses (H_e represents exit height), and Figure 4.2 compares the boundary layer thickness on both sides as a function of distance from the throat.

Table 4.2 - Comparing Non Blowing and Blowing Sides of Nozzle

Side	Thickness (t)	$t / (H_e/2)$	Error
Non Blowing			
Thickness	0.533 mm (.021")	0.033	$\pm 3.25\%$
Blowing			
Thickness	1.67 mm (.066")	0.103	$\pm 3.23\%$

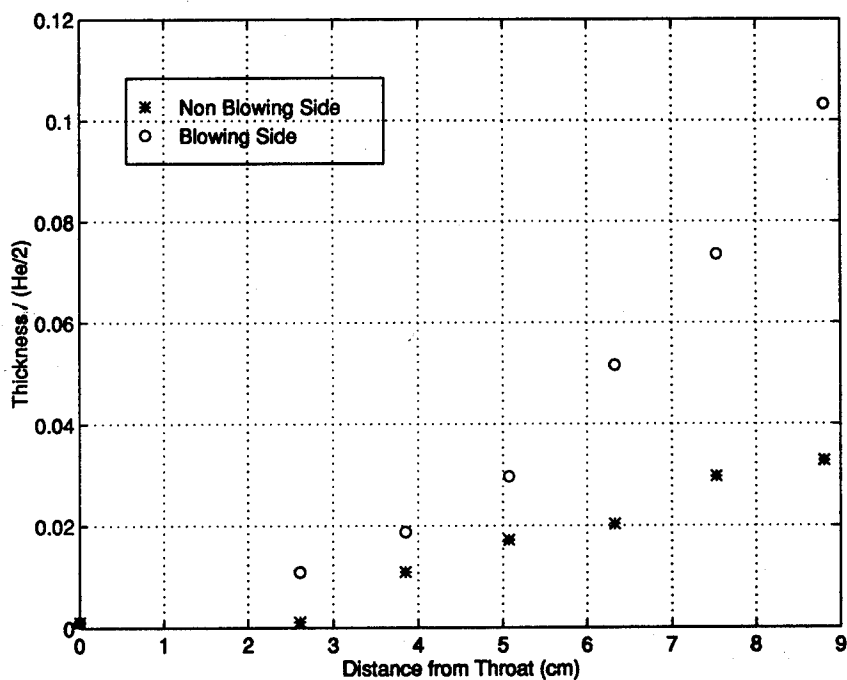


Figure 4.2 - Thickness vs Distance From Throat for Baseline Case

Clearly, the mere presence of a rough porous wall had an effect on the boundary layer, but this was not a true baseline case. Evidence that the roughness of the porous material was the major cause of boundary layer growth in the baseline case is provided by calculating k^+ . This value is a Reynolds number based on the average roughness of the surface. Taking the average roughness to be on the order of the porosity of the material (2 micron porosity), k^+ was calculated to be 76 at the throat and 58 at the exit. When k^+ is greater than 60, the surface is considered to be fully rough, which means that, in this case, the surface was fully rough over almost the entire porous surface. Based on this evidence, roughness of the porous material was the major contributor to boundary layer growth in the baseline case. It must be stated here, however, that a true baseline case was not observed in the experiment, and this also had an effect on the baseline results.

When there was not active injection through the porous material, the plenum pressure was equal to atmospheric pressure. The pressure gradient still existed in the nozzle during a run so pressure drops still occurred through the porous material. Therefore, even without active injection, there was a very small amount of suction near the throat of the nozzle where the wall pressure was greater than atmospheric and a very small amount of blowing near the end of nozzle ($B=.000128\pm7.2\%$) as the wall pressure dipped below atmospheric. Both of these effects could also have contributed to the boundary layer growth on the blowing side.

The presence of suction and blowing in the baseline case with no active injection implies that blowing was always greatest near the end of the nozzle where the pressure drop was greatest and cooling was needed least. Lack of flow control through porous material is a major criticism of transpiration cooling (May and Burkhardt, 1991:1), and it certainly was illustrated here because

maximum blowing near the exit affected the boundary layer thickness results of this experiment. While these measurements and observations point out the differences between the two sides of the nozzle, they also point out that even under baseline conditions, the boundary layer over a porous plate is a complex phenomenon.

In a rocket nozzle with porous nozzle walls, the boundary layer would be thicker than if the walls were impermeable as shown here. Therefore, additional boundary layer growth in the blowing cases of the experiment was measured relative to the baseline blowing side boundary layer thickness.

4.1.5 Exit Mach Number Profile

Exit Mach number is a measure of performance because it is directly related to exit velocity. Also, a uniform exit Mach number profile means uniformly axial exit flow, which is desired for wind tunnels. Exit Mach data was collected with a pitot probe placed at several positions across the exit plane.

The exit Mach number profile was calculated by averaging the total pressure ratio (p_{02}/p_{01}) in front of the pitot probe over the run time, and calculating Mach number using the gas dynamic equations (1953:623). Table 4.3 summarizes the results.

Table 4.3 - Summary of Baseline Exit Mach Number Data

Position	Mach Number	Error
Average across profile	1.886	$\pm 1.07\%$
Centerline	1.92	---
Avg in non blowing region	1.88	$\pm 2.18\%$
Avg in blowing region	1.88	$\pm 1.56\%$

The averages referred to in Table 4.3 and throughout this report refer to spatial averages across the exit plane, not the average over several runs. Therefore, these parameters were chosen because they were, statistically, better indicators of the effects of blowing on exit Mach number than a single data points near the walls. The non blowing and blowing regions were defined such that all data points from the centerline to the respective wall excluding centerline data points were included in the calculation of the average Mach number. The choice of these parameter resulted in a symmetric distribution across the exit plane in the original baseline case (Table 4.3).

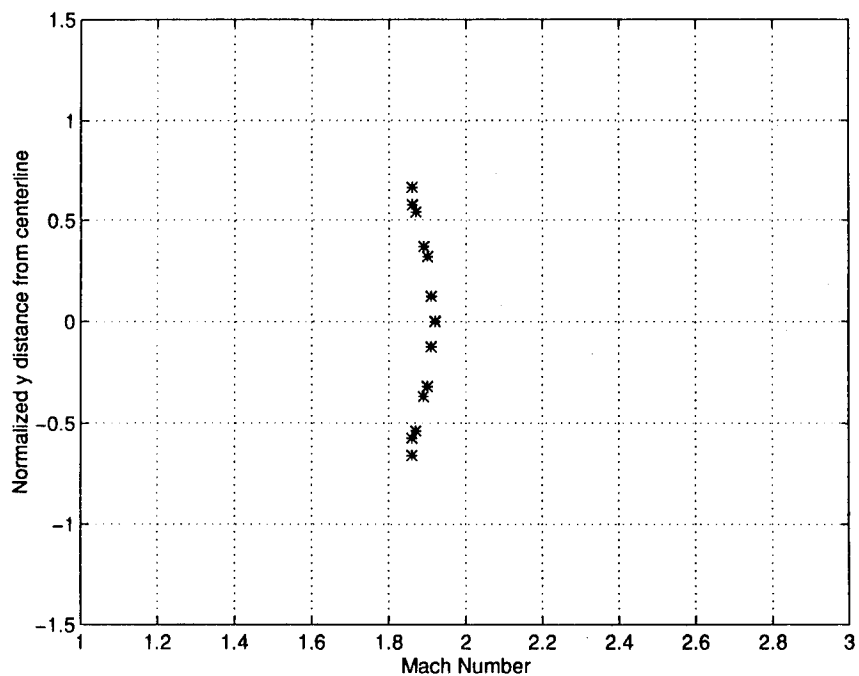


Figure 4.3 - Baseline Exit Mach Number Profile

As mentioned earlier, the baseline data did not represent a true baseline case, which would have required a nozzle with two impermeable walls. The suction and blowing present in the baseline case did slightly affect the baseline exit Mach number profile. A true baseline case was created by assuming that the Mach number profile near the non blowing wall would be the same

near any impermeable wall. The data near the non blowing wall was mirrored above and below the nozzle centerline to create a true baseline case for exit Mach number profile. Therefore, six exit Mach number cases are represented here: one baseline and five with blowing. The blowing case that had no active injection is referred to as the Blowing 0 case for the remainder of this report. The new baseline exit Mach number profile using the mirrored data is shown in Figure 4.3.

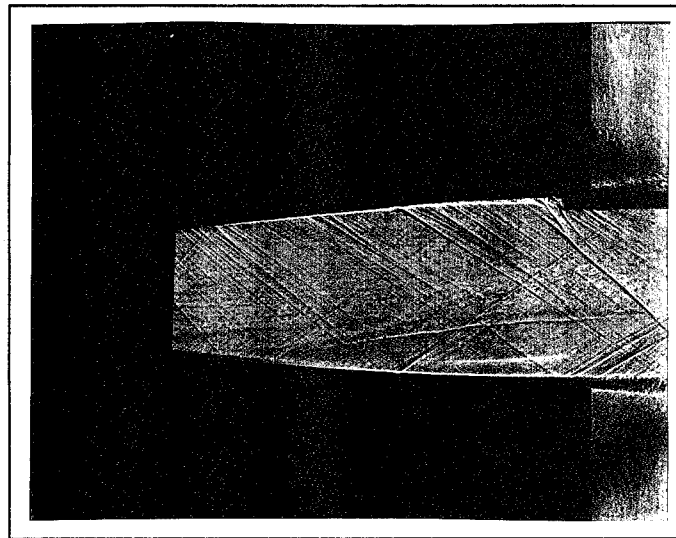


Figure 4.4 - Pitot Probe as Part of the Wall

Many more data points were taken for the baseline case than for the blowing cases because a very complete picture of the baseline exit Mach number profile was desired. Also, decreases in exit Mach number with blowing were expected to occur most dramatically near the walls so less freestream data points were deemed necessary. Unfortunately, the pitot probe was necessarily large compared to the exit height of the nozzle, which made fine measurements inside the boundary layer itself impossible. In fact, the probe had to be placed at least 3.37mm (0.1328")

from the wall or the wall/probe interaction contaminated the pitot pressure measurements (See Figure 4.4). Therefore, data for exit Mach number immediately next to either wall was not acquired.

4.2 Blowing Cases

4.2.1 Definition

Four cases with active injection were studied, and they were defined by the target plenum pressure used in each case. The minimum plenum pressure (259 kPa) was the lowest possible pressure that produced positive blowing along the entire porous area. The maximum plenum pressure was set based on hardware limitations.

A regulator was necessarily connected to the air bottle used for injection, and even with it and the air bottle completely open, the regulator was mass flow limited. Therefore, the plenum pressure could only be maintained at 382 kPa, which became the maximum plenum pressure. The other plenum pressures were chosen so that the intermediate cases would be evenly spaced between the minimum and maximum plenum pressures. The test plenum conditions were very repeatable at each blowing level, and the variations in the plenum conditions were small enough to have very little effect on the blowing ratios. Table 4.4 summarizes the blowing conditions. The Blowing 0 case was included here because blowing was present at atmospheric plenum conditions, which made it the limiting case of blowing as mentioned earlier.

Blowing ratios were calculated by Eq.1-1 with program BLOWDOT.FOR in which mass flow rates were calculated, converted to the blowing parameter, and summed at increments along the porous area. Calculations were based on the actual x-y coordinates of the nozzle, measured

static pressure at each coordinate, and plenum conditions. Each increment was centered around an x coordinate so that the summation is more accurate. Only positive blowing was considered in the blowing ratio, but the suction mass flow rate was also calculated for later analysis. Table 4.5 summarizes the blowing ratios obtained in this experiment.

Table 4.4 - Summary of Blowing Conditions

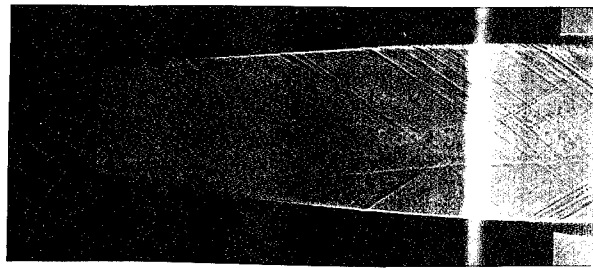
Case	Plenum Pressure	Error	Plenum Temp	Error
Blowing 0	98.5 kPa (14.29 psi)	$\pm 0.09\%$	295.18 K	$\pm 0.04\%$
Blowing 1	259 kPa (37.63 psi)	$\pm 1.19\%$	291.53 K	$\pm 1.10\%$
Blowing 2	314 kPa (45.57 psi)	$\pm 0.44\%$	288.62 K	$\pm 0.25\%$
Blowing 3	348 kPa (50.55 psi)	$\pm 3.85\%$	287.61 K	$\pm 0.35\%$
Blowing 4	382 kPa (55.36 psi)	$\pm 0.96\%$	288.48 K	$\pm 0.75\%$

Table 4.5 - Summary of Blowing Ratio at each Blowing Level

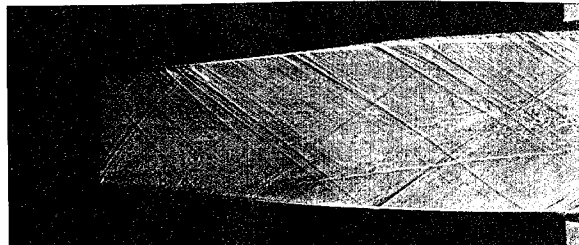
Case	Blowing Ratio	Error
Blowing 0	0.000128	$\pm 7.18\%$
Blowing 1	0.004640	$\pm 4.18\%$
Blowing 2	0.007695	$\pm 1.72\%$
Blowing 3	0.009853	$\pm 16.9\%$
Blowing 4	0.011552	$\pm 4.32\%$

4.2.2 Boundary Layer Growth

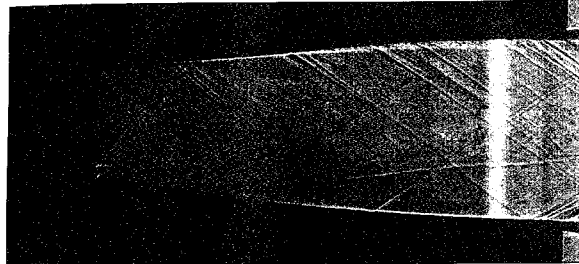
Visualization of the boundary layer at each blowing level gave the first indication that transpiration cooling had an effect on boundary layer thickness. Figure 4.5 shows a series of shadowgraphs taken at approximately the same time for each blowing level. Notice that the boundary layer on the non blowing wall is unchanged from the non blowing case as it should be (compare with Figure 4.1c), but the increase in boundary layer thickness on the blowing side with



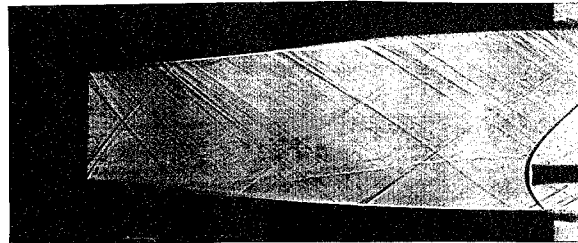
(a) Blowing 0



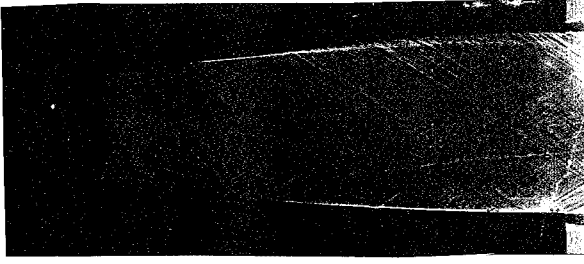
(b) Blowing 1



(c) Blowing 2



(d) Blowing 3



(e) Blowing 4

Figure 4.5 - Shadowgraphs Showing Boundary Layer at Each Blowing Level

increasing blowing is clearly visible. All other visible features of the flow including mach lines and local turbulence patterns appear to be unchanged in each case indicating that the disturbance due to transpiration was limited to the boundary layer.

As mentioned, boundary layer growth was evaluated as a ratio of boundary layer thickness to exit height, and this evaluation was accomplished considering only one side and half the exit height. The values would be the same if it were assumed that both sides were transpiration cooled and the entire exit height was considered. Table 4.6 gives the measured exit boundary layer thicknesses, and Figure 4.6 shows the boundary layer growth data in terms of comparison with percent growth.

Table 4.6 - Summary of Boundary Layer Growth Data

Case	Exit b.l. thickness,	Error	$t / (H_e/2)$	Growth
Non Blowing	1.68 mm (0.066")	3.2%	0.103	0.0%
Blowing 1	1.93 mm (0.076")	3.6%	0.119	15.5%
Blowing 2	2.16 mm (0.085")	2.8%	0.133	29.1%
Blowing 3	2.29 mm (0.090")	4.0%	0.141	36.8%
Blowing 4	2.46 mm (0.097")	2.7%	0.152	47.5%

A quadratic curve was fit to this data because this could be useful for interpolation between the data points at this range of blowing ratios. It is unknown if this curve fit would apply to data outside this range of blowing ratios, but it seems unlikely that the boundary layer thickness would continue to increase at its current rate for long without leveling off.

Boundary layer thickness growth data along the nozzle did not show the jump in thickness at the beginning of the porous material reported by Goldstein et.al., but there is a good reason for

this. Goldstein's experiment involved a flat plate with no pressure gradient so there was constant blowing over the entire porous section. In that case, when the flow interacted with the injection there was a significant jump in boundary layer thickness (See Figure 1.3). Because of the pressure gradient present in this experiment, the blowing ratio starts small and increases along the porous area. This causes a smooth, blended growth along the length of the nozzle, and this type of disturbance in the boundary layer, as opposed to the abrupt disturbance caused by film cooling or cases with no pressure gradient, strengthens the case for transpiration cooling.

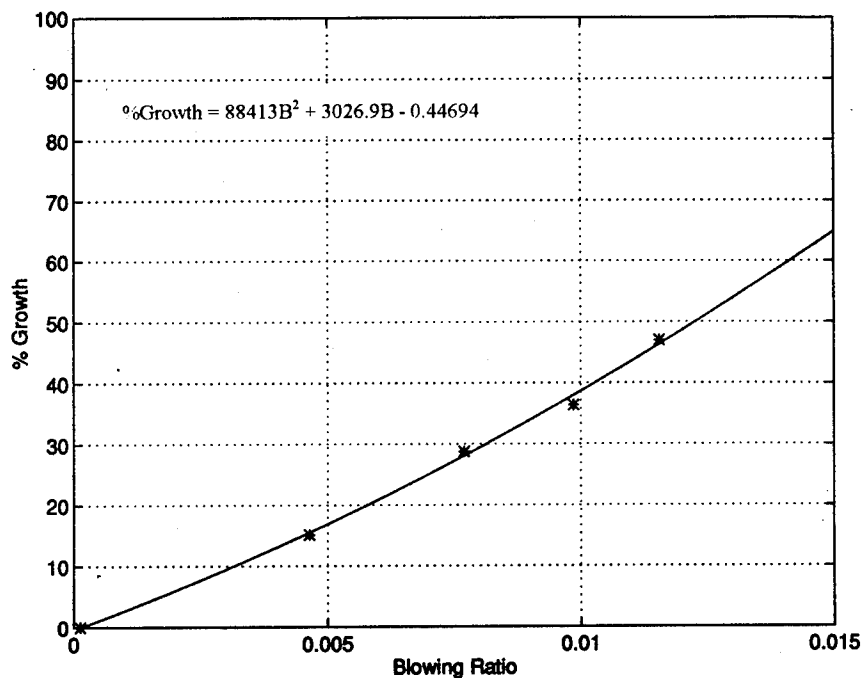


Figure 4.6 - Blowing Ratio vs Boundary Layer Growth

Goldstein's lowest blowing ratio (0.0078) was the most similar to those used in this experiment, and he showed approximately a 60% increase in boundary layer thickness, which is larger than the growth seen here (see Figure 4.6). This is immediately seen as a benefit of

transpiration cooling. The smooth transition can be seen from the shadowgraphs (See Figure 4.5), and the data in Figure 4.7.

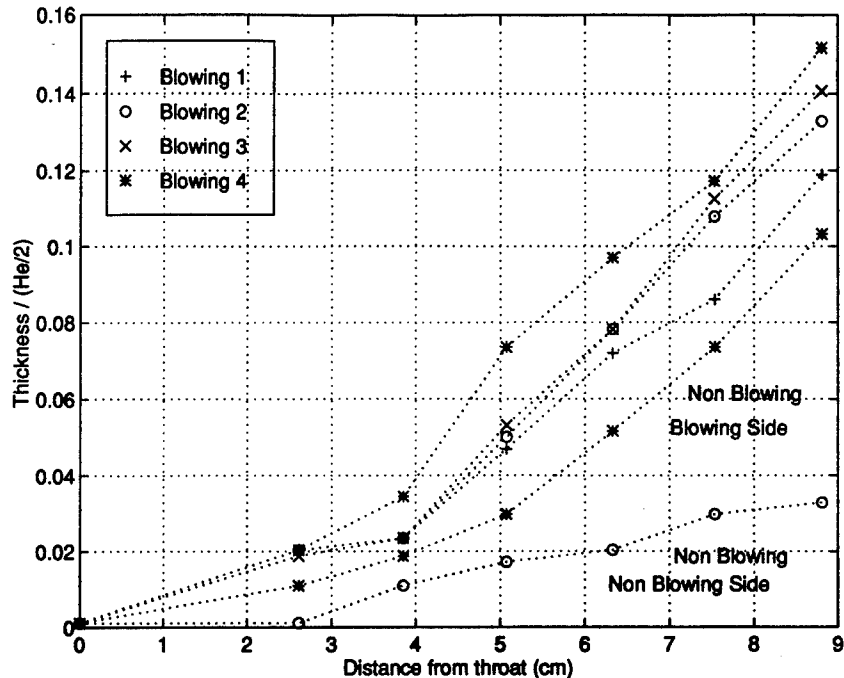


Figure 4.7 - Boundary Layer Growth vs Distance from Throat

4.2.3 Wall Mach Number

The Mach number along the wall was measured based on static pressure for several runs at each blowing level to determine if blowing had a noticeable effect on wall Mach number. There were small differences observed when comparing the Mach numbers on the two sides, and several factors such as roughness and the laminar sublayer thickness could have contributed to this difference. Of more interest was the fact that the difference was the same at every blowing level. All wall Mach number data points collected were plotted in Figures 4.8, but the data was so constant that several data points fell on top of one another. The same was true when the Mach number data was converted to pressure ratios in Figure 4.9. Therefore, it can be seen that

blowing had no effect on wall Mach number at any blowing ratio. Because blowing did not affect the wall static pressure, assuming a thin boundary layer for analysis of the transpired boundary layer appears to remain a valid at low blowing ratios.

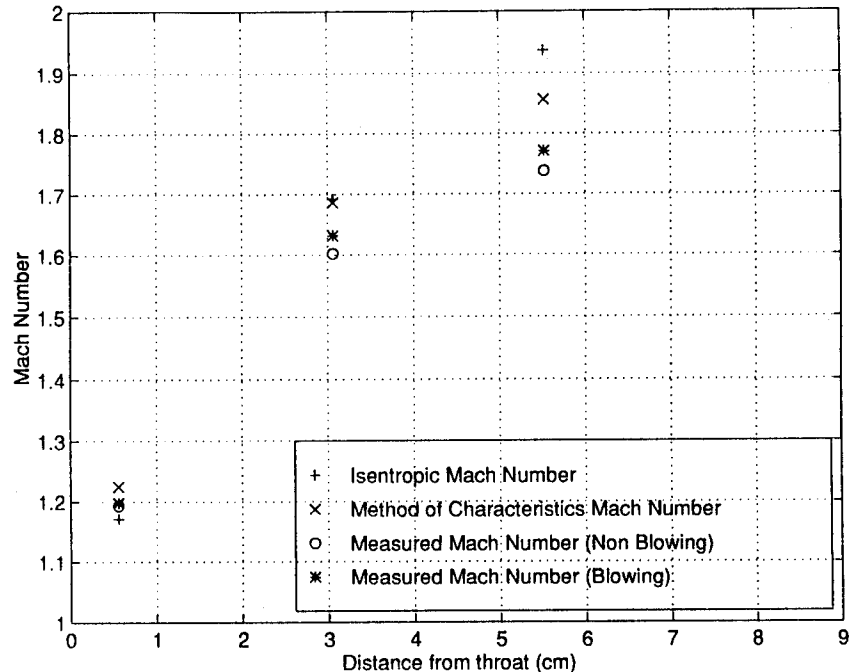


Figure 4.8 - Mach Number vs Distance from Throat

Also, the quality of the model was seen from the small differences between the measured static pressures and wall Mach numbers and the exact characteristic solutions for the nozzle. These differences were expected and were attributed to the manufacture of the model. This result also shows that blowing at low blowing ratios does not have major effects on the flow field of the nozzle.

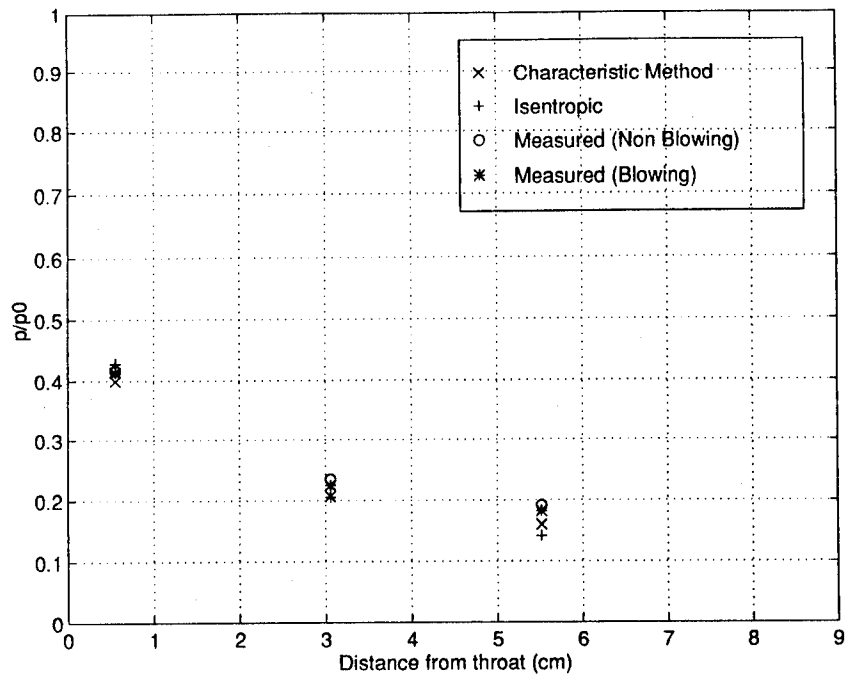


Figure 4.9 - Pressure Ratio vs Distance from Throat

4.3 Performance

4.3.1 Exit Mach Number

Boundary layer growth with injection has already been shown, which increased the mass flow defect region in the boundary layer. Therefore, more of the flow energy had to be spent to accelerate the very low velocity injected gas and overcome this defect. This loss of energy was expected to degrade the exit Mach number especially near the wall. Larger injection rates cause greater disturbances to the flow. When exit flow is not uniform in a wind tunnel, it approximates freestream flow less accurately, and this introduces greater error into the wind tunnel data. For transpiration to be an attractive method of cooling high temperature wind tunnels, this effect must be quantified.

Mach numbers were determined in the same way as the baseline case, but less points per case were taken. Data points near the walls were more important in the blowing cases because the effects were expected in those regions. The centerline exit Mach number was also measured as a reference for each blowing level. Figure 4.10 compares the exit Mach profile for each case with the baseline case (see Figure 4.3), and Table 4.7 summarizes the data.

The maximum error in the Mach number data presented in Figure 4.10 was $\pm 2.87\%$ so there is high confidence in the pitot probe measurements. Errors in the average non blowing and blowing Mach numbers were expected because the Mach number did vary from the centerline to the wall, and with a small number of data points, the errors tended to be large. This was still a better indication of the effect of transpiration on each side of the nozzle than a single data point near the wall.

Table 4.7 -Summary of Exit Mach Number Data

Case	Avg	Error	Centerline	Non Blowing Avg	Error	Blowing Avg	Error
Non Blowing	1.886	$\pm 1.06\%$	1.92	1.882	$\pm 1.54\%$	1.884	$\pm 2.17\%$
Blowing 1	1.884	$\pm 2.76\%$	1.91	1.900	--	1.870	$\pm 7.43\%$
Blowing 2	1.860	$\pm 1.77\%$	1.88	1.870	$\pm 34.0\%$	1.847	$\pm 4.54\%$
Blowing 3	1.862	$\pm 2.42\%$	1.90	1.870	$\pm 34.0\%$	1.843	$\pm 6.99\%$
Blowing 4	1.848	$\pm 3.08\%$	1.88	1.875	$\pm 42.4\%$	1.820	$\pm 7.63\%$

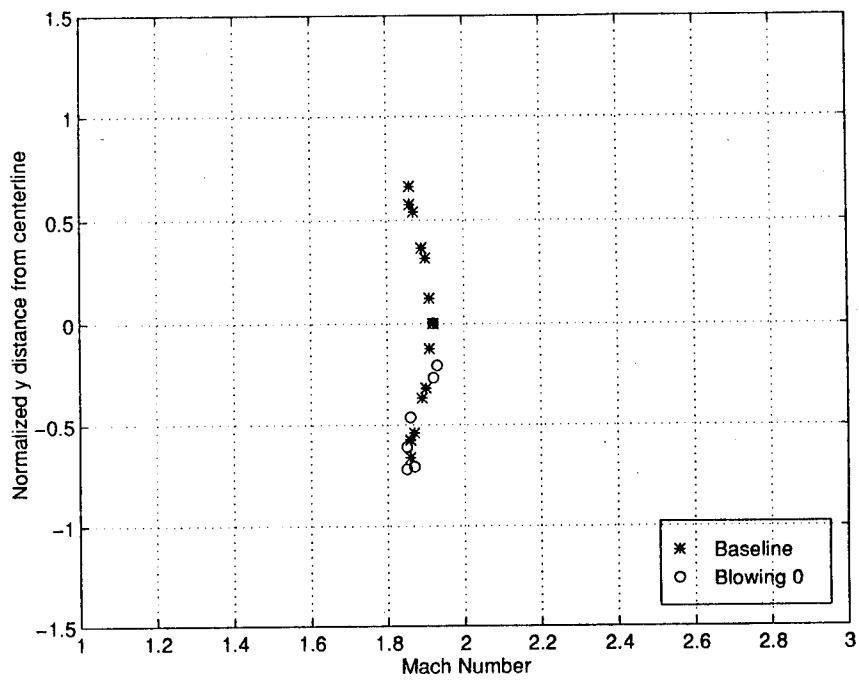


Figure 4.10a - Baseline and Blowing 0

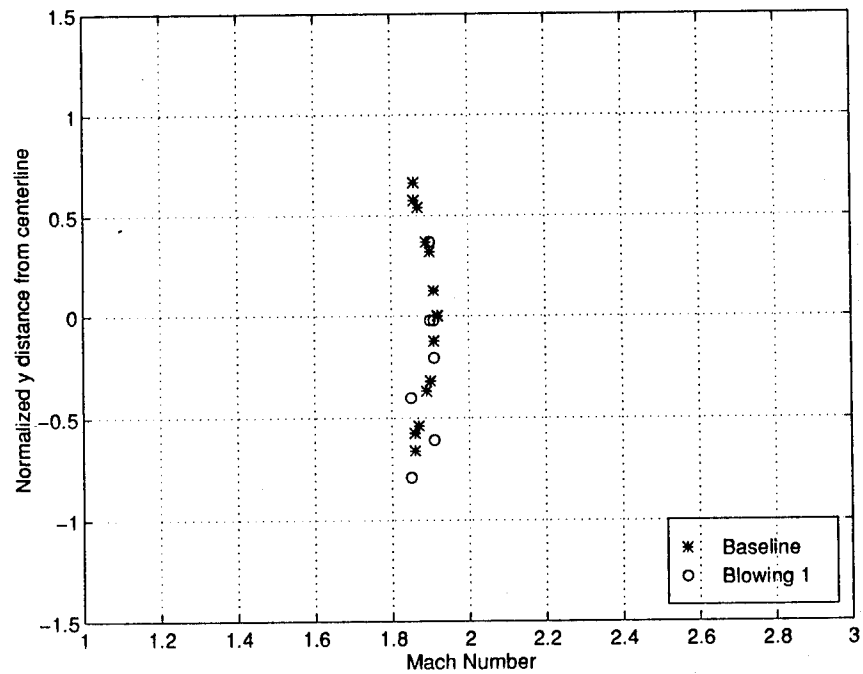


Figure 4.10b - Baseline and Blowing 1

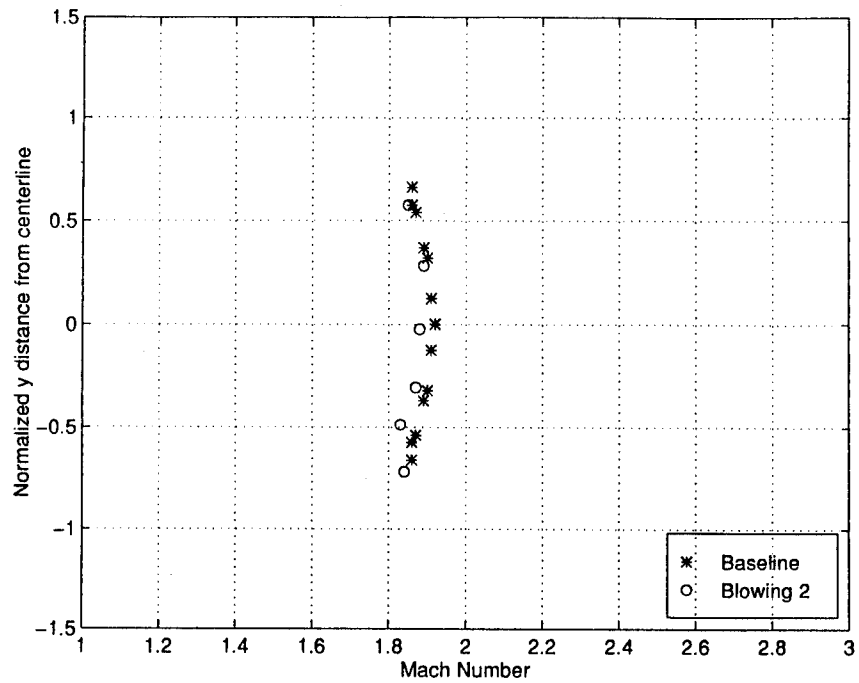


Figure 4.10c - Baseline and Blowing 2

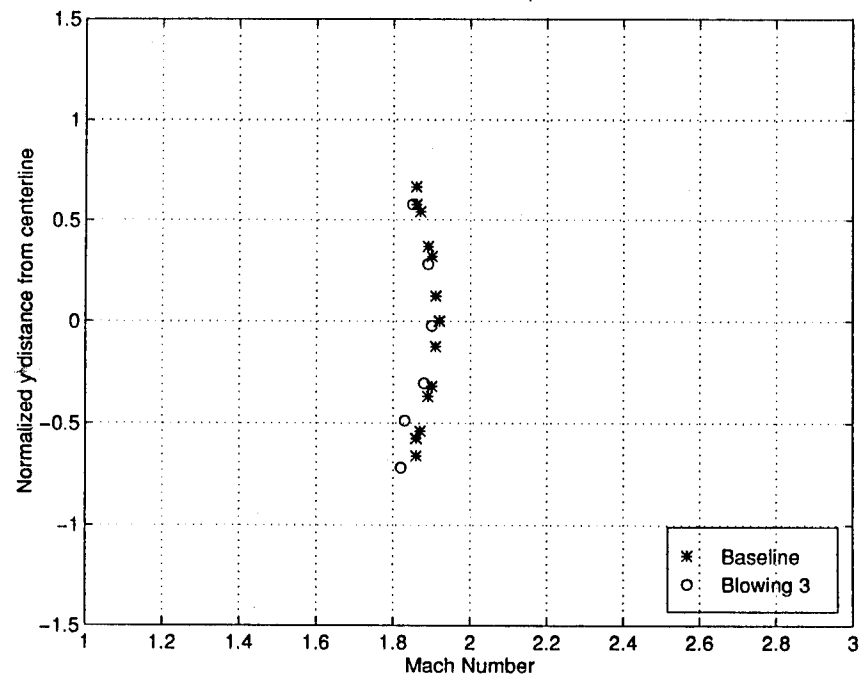


Figure 4.10d - Baseline and Blowing 3

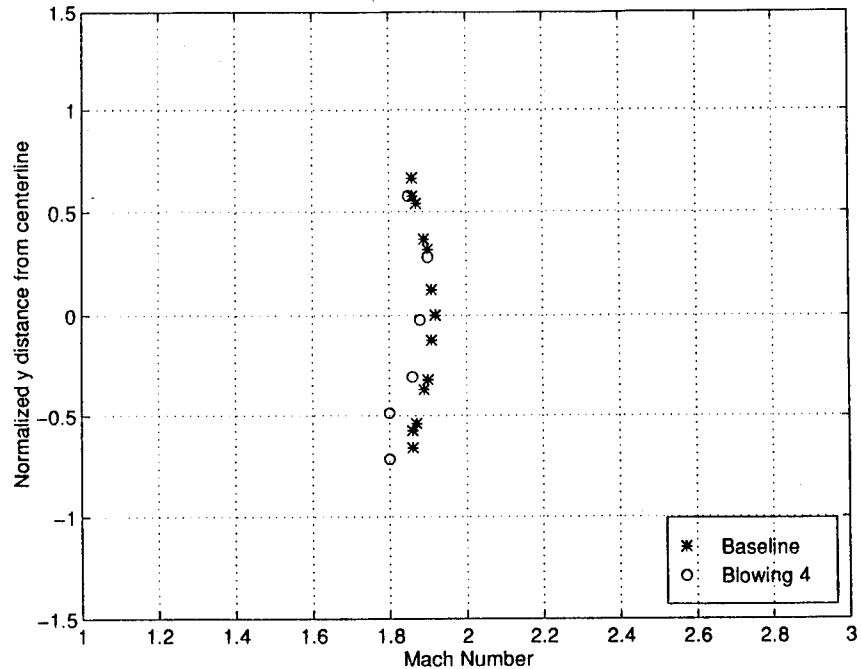


Figure 4.10e - Baseline and Blowing 4

The effects of transpiration on the exit Mach number were small in this study, -2% in overall average Mach number, and -3.4% in the blowing region. The average Mach number in the blowing region stayed within 2% of the centerline Mach number. These results confirmed that transpiration would decrease the exit Mach number of the nozzle and also showed that the effect of transpiration was limited to the blowing region. The decrease in exit Mach number had an adverse effect on the performance of the nozzle because Mach number is directly related to exit velocity. In Figure 4.11, the exit Mach number parameters used in this experiment are shown relative to the design Mach number, 2.0, against blowing ratio to visualize the effects of transpiration.

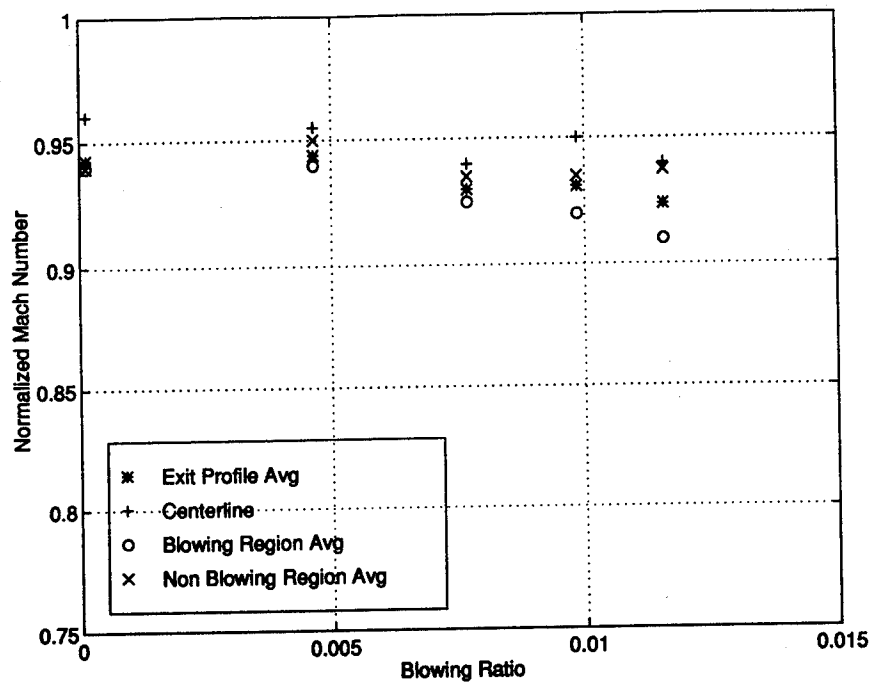


Figure 4.11 - Exit Mach Number Trends vs Blowing Ratio

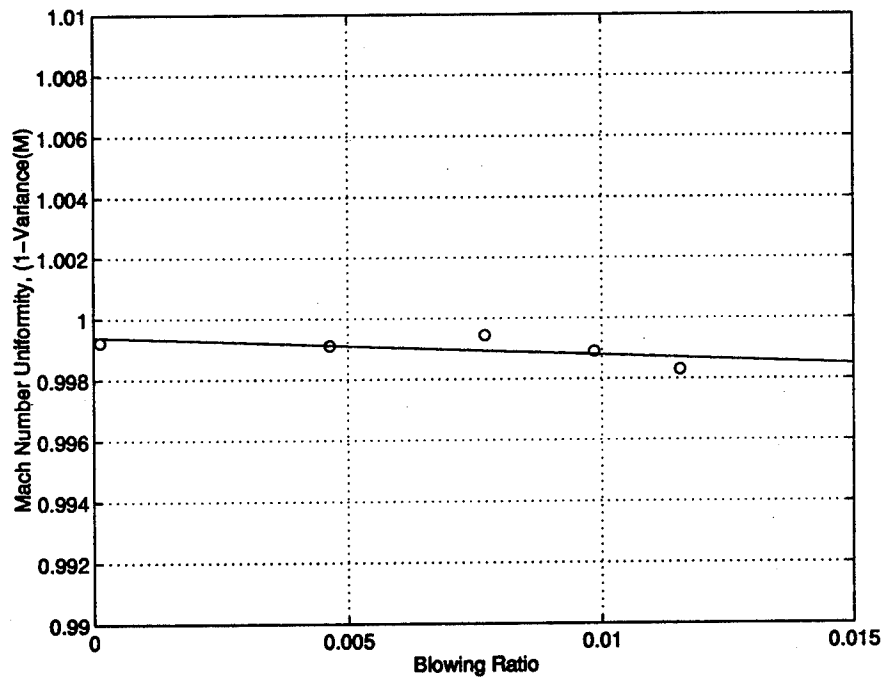


Figure 4.12 - Decrease in Uniformity w/ Blowing

The other effect of decreased exit Mach number near the walls (indicated by blowing average Mach number), was decreased uniformity of the exit flow. The importance of flow uniformity to wind tunnels has already been stated, but it is also a concern for thrust. Non uniform exit flow has velocity components perpendicular to the exit plane, which decrease thrust. Figure 4.12 uses the quantity (1 - spatial variance of the exit flow) to show the decrease in uniformity with increased blowing.

4.3.2 Specific Impulse

In rocket engine design, an important performance parameter is specific impulse or I_{sp} . It is a measure of fuel consumption efficiency because it is related to mass flow rate and thrust by Eq.4-1.

$$I_{sp} = \frac{\dot{m}u_e + A_e(p_e - p_a)}{\dot{m}g_0} \quad (4-1)$$

where: \dot{m} = mass flow rate

u_e = exit velocity

A_e = exit area

p_e = exit pressure

p_a = ambient pressure

It was expected that transpiration, while adding mass flow to the nozzle, would degrade the I_{sp} of the nozzle slightly because of the exit Mach number decreases and the temperature of the injected gas.

Specific impulse was calculated as an extension of the blowing ratio analysis with BLOWDOT.FOR. Total mass flow rate took into account the mass flows due to suction and blowing. In every case except Blowing 0 the total mass flow taking into account suction and blowing was greater than the freestream mass flow rate. Calculations were originally made at the chamber conditions specific to each run, but the small variances from run to run caused the results to spread too much to be useful. Therefore, the data was normalized to the average chamber conditions, and a trend was noticeable from the results. Figure 4.13 shows the results.

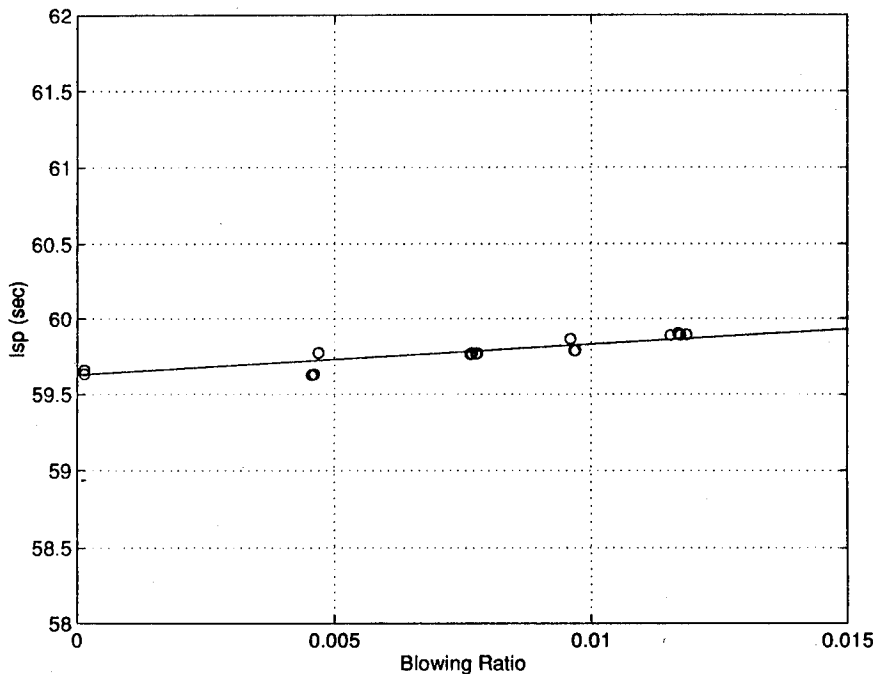


Figure 4.13 - Blowing Ratio vs Isp

From Figure 4.13 it can be seen that transpiration had virtually no effect on the specific impulse of the nozzle, and if anything, there is a slight upward trend. The effect was very small due to the transpiration setup in the nozzle. First of all, the blowing ratios were very small, which means that very little mass was injected into the flow. Also, most of the injection occurred near

the back of the porous area where the pressure drop was greatest. By the time the freestream air reached that point it had cooled to a temperature that was very close, and perhaps a little lower, than the injected air. Therefore, it was not cooling the freestream air, which would have been a source of performance loss in the nozzle. The combination of small losses in exit velocity and temperature combined with increased total mass flow and exit pressure acted to cancel each other out in this case. The canceling of these trends resulted in the negligible effect on the nozzle's performance. As an example of the counteracting trends, Figure 4.14 shows how thrust increased slightly more rapidly than total mass flow rate at higher blowing ratios.

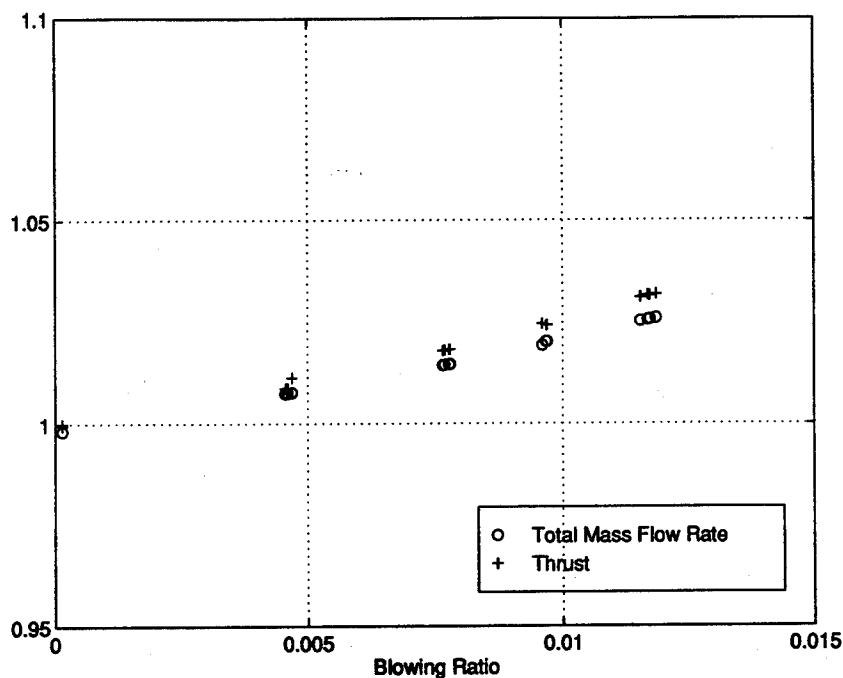


Figure 4.14 - Blowing Ratio vs Thrust, Mass Flow Rate, Exit Temp, and Exit Pressure

V. Conclusions and Recommendations

The objectives of this study were to understand the differences between flow over a porous and non porous wall with no blowing, to relate blowing ratio to boundary layer thickness on a porous wall, to relate blowing ratio to the uniformity and magnitude of the exit Mach number, and relate the above results to the performance of the nozzle. All of these objectives were met, and some additional conclusions and recommendations were also made.

The boundary layer was shown to be 213% greater on the blowing side of the nozzle than on the non blowing side, but this difference did not affect the exit Mach number. The conclusion, then, is that in this case, the boundary layer growth due to the porous wall without blowing was caused mostly by the roughness of the material. Even without active injection, however, suction and blowing along the nozzle due to the pressure gradient was present. All of these effects together pointed out that the boundary layer over a porous wall without active injection was still very complex.

At low blowing ratios, the blowing side boundary layer thickness showed significant increases over the non blowing case as expected. The boundary layer thickness increased by as much as 47% over the small range of blowing ratios studied, which made the boundary layer thickness increase function steep at low blowing ratios. The increase along the wall was continuous, however, which means that the injection caused a smooth, blended flow disturbance along the wall, and this is a benefit to transpiration cooling over film cooling.

Exit Mach number was adversely affected by blowing. The average exit Mach number decreased by 2%, but more importantly, the average Mach number in the blowing region decreased by 3.4%. Therefore, low blowing ratios have a noticeable effect on the exit flow of a

nozzle, and if the entire nozzle were transpiration cooled, the effects would be would have been greater. The Mach number profile across the exit plane was also disrupted in terms of uniformity, as shown by a 50% increase in the variance of the exit profile. Therefore, transpiration cooling also has a noticeable effect on exit flow uniformity low blowing ratios.

Performance calculations showed that transpiration cooling caused a slight upward trend in the specific impulse of the nozzle. The trend, however, was so slight that it can be concluded that at the low blowing ratios and low thrust chamber temperatures studied in this experiment, transpiration cooling had no effect on the performance of the nozzle in terms of specific impulse. This conclusion is attributed to factors including porous area geometry and the temperature range of the experiment. If this had been a combustion experiment with extremely high temperature in the nozzle there almost certainly would have been a decrease in performance. If an application for a low temperature nozzle is found, however, transpiration cooling might prove useful for more than cooling.

The geometry of the blowing area had two effects on this experiment that brought to light one of the major criticisms of transpiration cooling, lack of flow control in the presence of a pressure gradient. During this experiment, most of the blowing occurred at the aft end of the porous area because the flow tended to go where the pressure was lowest, and this effect caused three problems. First, blowing was concentrated away from the throat where it was needed most. Second, the exit boundary layer was probably thicker than it would have been had blowing been concentrated at the throat, and lastly, the temperature of the injected gas was the same or higher than the freestream gas, which reduced the effect of injection on performance. Therefore, unless

a variable porosity material becomes readily available, the porous area in the presence of a pressure gradient should be such that these effects are reduced.

The problem should not be approached with wild abandon, however, because it is unclear what combination of effects will occur when the porous area is concentrated. The porous area should not be so concentrated as to negate the transitional flow disturbance benefit of transpiration. If this occurs then transpiration cooling approximates film cooling, and this may not be desirable. The only certain thing about concentrating the porous area is that the injection will be applied at the throat where it is needed. Therefore, changing the porous material injection geometry is a logical extension of this research.

Two recommendations for future research are made. First, more data of the kind presented here should be taken at higher blowing ratios to extend the present curves because it is expected that the trends established here will continue at higher blowing ratios. This would provide a more complete picture of the effects of transpiration cooling. Secondly, the porous area geometry should be changed and a complete set of curves be created to compare with these. This comparison should point to the transpiration setup that provides the best cooling effectiveness with the smallest performance loss.

Heat transfer was shown in a parallel study by Captain Joseph Lenertz to have been reduced by 14% in the same nozzle used here, which is significant considering the low blowing ratios studied in this experiment. Major performance losses were not observed in this experiment but were proportional to the amount of injection, and based on the amount of heat transfer reduction observed in the parallel study, a clear trade off exists between heat transfer reduction

and performance loss. Overall, then, transpiration cooling was shown to have potential as an effective means of cooling with minimal performance loss in nozzle applications.

Bibliography

Antonia, R.A. and Fulachier, L. "Topology of a turbulent boundary layer with and without wall suction." Journal of Fluid Mechanics. 198 (1989): 429-435.

Azevedo, David. "Measured Thrust Losses Associated with Secondary Air Injection Through Nozzle Walls." Journal of Propulsion and Power. 9 (1993): 43-50.

Bartz, D.R. "An Approximate Solution of Compressible Turbulent Boundary-Layer Development and Convective Heat Transfer in Convergent-Divergent Nozzles." Transactions of the ASME. November, 1995: 1235-1245.

Bowersox, Dr. Rodney, SHOCKTUN. Vers. 1.0. Computer software. Personal, 1990. Fortran 77.

-----, NOZ2. Vers. 1.0. Computer software. Personal, 1990. Fortran 77.

-----, BLCORR. Vers. 1.0. Computer software. Personal, 1990. Fortran 77.

-----, WALL., Vers. 1.0. Computer software. Personal, 1990. Fortran 77.

Goldstein, R.J., Shavit, G., and Chen, T.S. "Film Cooling Effectiveness With Injection Through a Porous Section." Journal of Heat Transfer. August 1965:353-360.

May and Burkhardt. "Transpiration Cooled Throat for Hydrocarbon Rocket Engines." NASA CR 8-36952. December, 1991: 1-53.

Schetz, Joseph A. Foundations of Boundary Layer Theory. Prentice-Hall, Inc.:Englewood Cliffs, NJ, 1984.

Schlichting, Dr. Hermann. Boundary Layer Theory. McGraw-Hill Book Company:New York, 1968.

Shapiro, Ascher H. The Dynamics and Thermodynamics of Compressible Fluid Flow. 2 vols. New York:John Wiley and Sons, 1953-54.

Simpson, Roger L., Moffat, R.J., and Kays, W.M. "The Turbulent Boundary Layer on a Porous Plate: Experimental Skin Friction With Variable Injection and Suction." International Journal of Heat and Mass Transfer. 12 (1969): 771-789.

Kays, W.M. and Crawford, M.E. Convective Heat and Mass Transfer. McGraw-Hill Book Company: New York, 1980.

White, Frank M. Viscous Fluid Flow. McGraw-Hill, Inc.:New York, 1991.

Zuppan, Lawrence L. Maj. An Investigation of the Variation of Throat Height on the Performance of Convergent-Divergent Nozzles in a Shock Tube. MS Thesis AFIT/GAE/ENY/Dec 1964. School of Engineering, Air Force Institute of Technology, Wright-Patterson AFB, OH, December 1964.

APPENDIX A
Gamma Calculation for air/He Driver

A.1

APPENDIX A - γ Calculation for He/Air Driver Mixture

Given: $T_\infty = 294.43 \text{ K}$

$$R_{air} = 287 \text{ J/kg-K}$$

$$m_{He} = 4 \text{ kg/mol}$$

$$\gamma_{air} = 1.4$$

$$\gamma_{He} = 1.667$$

Find c_p and c_v for air (Hill and Peterson, p.38):

$$c_{p1} = 1004.26 \text{ J/kg}^\circ\text{K}$$

$$c_{v1} = 717.26 \text{ J/kg}^\circ\text{K}$$

Find c_p and c_v for He:

$$R_{He} = \frac{8314.3 \frac{J}{kg - K}}{4 \frac{kg}{mol}} = 2078.5 \frac{J}{kg - K}$$

$$c_{p2} = c_{v2} + R_{He}$$

$$c_{v2} \cdot \gamma_{He} = c_{v2} + R_{He}$$

$$c_{v2} = \frac{R_{He}}{(\gamma_{He} - 1)}$$

$$c_{v2} = \frac{2078.5 \frac{J}{kg - K}}{(1.667 - 1)} = 3116.19 \frac{J}{kg - K}$$

$$c_{p2} = 3116.19 \frac{J}{kg - K} + 2078.5 \frac{J}{kg - K} = 5194.69 \frac{J}{kg - K}$$

Find densities of each gas in the driver section:

$$p = \rho RT$$

$$\rho = \frac{p}{RT}$$

$$\rho_{air} = \frac{14.4 \text{ psi}}{(287 \frac{J}{kg - K})(294.3K)} = \frac{99284.5 \text{ Pa}}{(287 \frac{J}{kg - K})(294.3K)} = 1.17494 \frac{kg}{m^3}$$

$$\rho_{He} = \frac{70.0 \text{ psi}}{(2078.5 \frac{J}{kg - K})(294.3K)} = \frac{482500.0 \text{ Pa}}{(2078.5 \frac{J}{kg - K})(294.3K)} = .78878 \frac{kg}{m^3}$$

Use density averaging method to find mixture c_p and c_v :

$$c_{vm} = \frac{\rho_{air} c_{v1} + \rho_{He} c_{v2}}{\rho_{air} + \rho_{He}} = \frac{(1.17494)(717.26) + (.78878)(3116.19)}{(1.17494 + .78878)} = 1680.853 \frac{J}{kg - K}$$

$$c_{pm} = \frac{\rho_{air} c_{p1} + \rho_{He} c_{p2}}{\rho_{air} + \rho_{He}} = \frac{(1.17494)(1004.26) + (.78878)(5194.69)}{(1.17494 + .78878)} = 2687.456 \frac{J}{kg - K}$$

$$\gamma_m = 1.598$$

$$R_m = 1006.6 \frac{J}{kg - K}$$

γ_m calculated above was the value used in shock tube calculations to find chamber conditions. This calculation was accomplished for a range of driver pressure mixtures to create the spreadsheet shown on page A.4.

Spreadsheet for calculating γ over a range of driver mixtures

Air Properties

$$R = 287 \text{ J/kg-K}$$

$$c_p = 1004.26 \text{ J/kg-K}$$

$$c_v = 717.26 \text{ J/kg-K}$$

Helium Properties

$$R = 2078.5 \text{ J/kg-K}$$

$$c_p = 5194.69 \text{ J/kg-K}$$

$$c_v = 3116.19 \text{ J/kg-K}$$

Gas Temperature = 294.3 K

Air Pressure (psi)	Helium Pressure (psi)					
	70.00	70.50	71.00	71.50	72.00	72.50
14.00	1.6003	1.6006	1.6010	1.6013	1.6017	1.6020
14.05	1.6001	1.6005	1.6008	1.6012	1.6015	1.6018
14.10	1.5999	1.6003	1.6006	1.6010	1.6013	1.6017
14.15	1.5997	1.6001	1.6005	1.6008	1.6011	1.6015
14.20	1.5996	1.5999	1.6003	1.6006	1.6010	1.6013
14.25	1.5994	1.5997	1.6001	1.6005	1.6008	1.6011
14.30	1.5992	1.5996	1.5999	1.6003	1.6006	1.6010
14.35	1.5990	1.5994	1.5997	1.6001	1.6004	1.6008
14.40	1.5989	1.5992	1.5996	1.5999	1.6003	1.6006
14.45	1.5987	1.5990	1.5994	1.5998	1.6001	1.6004
14.50	1.5985	1.5989	1.5992	1.5996	1.5999	1.6003
14.55	1.5983	1.5987	1.5990	1.5994	1.5998	1.6001
14.60	1.5982	1.5985	1.5989	1.5992	1.5996	1.5999
14.65	1.5980	1.5983	1.5987	1.5991	1.5994	1.5998
14.70	1.5978	1.5982	1.5985	1.5989	1.5992	1.5996
14.75	1.5976	1.5980	1.5984	1.5987	1.5991	1.5994
14.80	1.5975	1.5978	1.5982	1.5985	1.5989	1.5992
14.85	1.5973	1.5976	1.5980	1.5984	1.5987	1.5991
14.90	1.5971	1.5975	1.5978	1.5982	1.5986	1.5989
14.95	1.5969	1.5973	1.5977	1.5980	1.5984	1.5987
15.00	1.5968	1.5971	1.5975	1.5979	1.5982	1.5986

APPENDIX B
Computer Resources

B.1

Program SHOCKTUN.FOR

Purpose: Use shock tube relations to predict stagnation conditions behind a shock wave after reflection from a straight wall.

Inputs: All inputs to SHOCKTUN.FOR are from the keyboard
Driver Length (ft)
Driver Pressure (psi), Temperature (K)
Driven Length (ft)
Driven Pressure (psi), Temperature (K)

Output: File, SHOCK.OUT

SHOCK TUBE SUMMARY

REGION 4 (DRIVER SECTION)

Driver Length(m) = 1.21921
Gamma 4 = 1.57415
T4(K) = 294.430
P4(atm) = 4.04082

REGION 1 (DRIVEN SECTION)

Driven Length(m) = 5.48647
Gamma 1 = 1.40000
T1(K) = 294.430
P1(atm) = 0.979592

PRESSURE RATIO

p4/p1 = 4.12500

SHOCK RESULTS

p2/p1 = 2.29375
Ms = 1.45222
Ws(m/s) = 499.479

REGION 2 (AFTER SHOCK)

up(m/s) = u2 = 218.866
T2/T1 = 1.28866
M2 = 0.560562

REGION 4 (LEADING EXPANSION)

Ue = -619.077
a3(m/s) = 556.246

REGION 3 (LEADING EXPANSION)

Uer = 775.111

REGION 5 (REFLECTED SHOCK)

Mr1 = 1.39138
Wr(m/s) = 324.386
p5/p2 = 2.09194
p5/p1 = 4.79839
p5/p4 = 1.16325
T5/T2 = 1.24914
T5/T1 = 1.60971

STAGNATION CONDITIONS

Pt(atm) = 4.70046
T5(K) = 473.946

TEST TIME

Shock time = 10.9844
 Pistion time = 25.0677
 Run time(ms) = 14.0833
 Time endwall expansion(ms) = 10.6207

Program NOZ2.FOR

Purpose: Construct a contoured nozzle shape for a given exit Mach number and geometry using the method of characteristics.

Inputs: All inputs to SHOCKTUN.FOR are from the keyboard
 Desired number of characteristic reflections (2 or 4)
 k, controls curvature of throat area (.2 - 1.0 recommended)
 Exit height (input only half the actual exit height in inches)
 Ratio of specific heats (γ)
 Desired exit Mach number

Outputs: File, NOZZ.OUT - contains table of characteristic results, which is that exact solution at each point in the characteristic lattice.
 Includes: x,y coordinates, Mach numbers, Mach angles

Char #	x	y/y _{throat}	M	θ	v	
1	0.00000E+00	0.10000E+01	0.10000E+01	0.34907E-01	0.00000E+00	0.15708E+01
2	0.29101E+00	0.10051E+01	0.11402E+01	0.37771E-01	0.37771E-01	0.10697E+01
3	0.31491E+00	0.10059E+01	0.11476E+01	0.40635E-01	0.40635E-01	0.10580E+01
4	0.33881E+00	0.10069E+01	0.11549E+01	0.43499E-01	0.43499E-01	0.10468E+01
5	0.36272E+00	0.10079E+01	0.11621E+01	0.46363E-01	0.46363E-01	0.10362E+01
6	0.38664E+00	0.10090E+01	0.11692E+01	0.49227E-01	0.49227E-01	0.10261E+01
7	0.41056E+00	0.10101E+01	0.11762E+01	0.52092E-01	0.52092E-01	0.10163E+01
8	0.43449E+00	0.10113E+01	0.11831E+01	0.54956E-01	0.54956E-01	0.10070E+01
9	0.45843E+00	0.10126E+01	0.11899E+01	0.57820E-01	0.57820E-01	0.99798E+00
10	0.48237E+00	0.10140E+01	0.11967E+01	0.60684E-01	0.60684E-01	0.98930E+00
11	0.50632E+00	0.10154E+01	0.12034E+01	0.63548E-01	0.63548E-01	0.98092E+00
12	0.53028E+00	0.10169E+01	0.12100E+01	0.66412E-01	0.66412E-01	0.97281E+00
13	0.55425E+00	0.10184E+01	0.12165E+01	0.69277E-01	0.69277E-01	0.96495E+00
14	0.57823E+00	0.10201E+01	0.12230E+01	0.72141E-01	0.72141E-01	0.95733E+00
15	0.60222E+00	0.10218E+01	0.12294E+01	0.75005E-01	0.75005E-01	0.94993E+00
16	0.62622E+00	0.10235E+01	0.12358E+01	0.77869E-01	0.77869E-01	0.94274E+00
17	0.65022E+00	0.10254E+01	0.12422E+01	0.80733E-01	0.80733E-01	0.93575E+00
18	0.67424E+00	0.10273E+01	0.12485E+01	0.83598E-01	0.83598E-01	0.92893E+00

File, WALL.OUT - contains coordinates of upper wall and exact solution wall Mach numbers

x	y	M
0.0000E+00	0.3735E+00	0.1000E+01
0.1087E+00	0.3754E+00	0.1140E+01
0.1176E+00	0.3758E+00	0.1148E+01
0.1266E+00	0.3761E+00	0.1155E+01
0.1355E+00	0.3765E+00	0.1162E+01
0.1444E+00	0.3769E+00	0.1169E+01
0.1534E+00	0.3773E+00	0.1176E+01
0.1623E+00	0.3778E+00	0.1183E+01
0.1712E+00	0.3782E+00	0.1190E+01
0.1802E+00	0.3787E+00	0.1197E+01
0.1891E+00	0.3793E+00	0.1203E+01
0.1981E+00	0.3798E+00	0.1210E+01
0.2070E+00	0.3804E+00	0.1217E+01
0.2160E+00	0.3810E+00	0.1223E+01
0.2249E+00	0.3817E+00	0.1229E+01
0.2339E+00	0.3823E+00	0.1236E+01
0.2429E+00	0.3830E+00	0.1242E+01
0.2518E+00	0.3837E+00	0.1248E+01
0.2608E+00	0.3845E+00	0.1255E+01
0.2698E+00	0.3852E+00	0.1261E+01
0.2788E+00	0.3860E+00	0.1267E+01
0.2878E+00	0.3868E+00	0.1273E+01
0.2968E+00	0.3877E+00	0.1279E+01
0.3058E+00	0.3885E+00	0.1285E+01
0.3148E+00	0.3894E+00	0.1292E+01
0.3238E+00	0.3904E+00	0.1298E+01
0.3328E+00	0.3913E+00	0.1304E+01
0.3418E+00	0.3923E+00	0.1309E+01
0.3508E+00	0.3933E+00	0.1315E+01
0.4499E+00	0.4048E+00	0.1315E+01
0.6864E+00	0.4321E+00	0.1467E+01
0.7140E+00	0.4353E+00	0.1478E+01
0.7413E+00	0.4384E+00	0.1489E+01
0.7683E+00	0.4416E+00	0.1500E+01
0.7950E+00	0.4446E+00	0.1511E+01
0.8214E+00	0.4477E+00	0.1522E+01
0.8477E+00	0.4507E+00	0.1533E+01
0.8739E+00	0.4538E+00	0.1545E+01
0.8999E+00	0.4568E+00	0.1556E+01
0.9258E+00	0.4598E+00	0.1567E+01
0.9517E+00	0.4628E+00	0.1578E+01
0.9776E+00	0.4658E+00	0.1589E+01
0.1003E+01	0.4687E+00	0.1600E+01
0.1029E+01	0.4717E+00	0.1611E+01
0.1055E+01	0.4747E+00	0.1622E+01
0.1081E+01	0.4777E+00	0.1633E+01
0.1107E+01	0.4807E+00	0.1644E+01
0.1133E+01	0.4837E+00	0.1656E+01
0.1159E+01	0.4867E+00	0.1667E+01
0.1185E+01	0.4897E+00	0.1678E+01

Program BLCORR.FOR

Inputs: Type of gas (air,He,H₂,N₂,O₂), from keyboard
 Chamber Pressure, from keyboard
 Chamber Temperature, from keyboard
 File, WALL.OUT - output from NOZ2.FOR

Outputs: File, PROPOFX.DAT - contains centerline data including Mach number, static pressure, temperature, density, flow velocity, and Reynolds number

x(in)	y(in)	Mach	p(psi)	T(K)	rho	u(m/s)	Rex	Res
0.000E+00	0.368E+00	1.00	41.	408.9	2.42	405.3	0.00E+00	0.00E+00
0.128E+00	0.370E+00	1.14	35.	389.4	2.14	450.9	0.14E+06	0.14E+06
0.139E+00	0.370E+00	1.15	34.	388.3	2.13	453.4	0.15E+06	0.15E+06
0.150E+00	0.371E+00	1.15	34.	387.3	2.12	455.6	0.16E+06	0.16E+06
0.160E+00	0.371E+00	1.16	34.	386.3	2.10	457.8	0.18E+06	0.18E+06
0.171E+00	0.372E+00	1.17	34.	385.3	2.09	460.0	0.19E+06	0.19E+06
0.181E+00	0.372E+00	1.18	33.	384.3	2.07	462.1	0.20E+06	0.20E+06
0.192E+00	0.373E+00	1.18	33.	383.3	2.06	464.3	0.21E+06	0.21E+06
0.202E+00	0.373E+00	1.19	33.	382.4	2.05	466.4	0.22E+06	0.22E+06
0.213E+00	0.374E+00	1.20	32.	381.4	2.03	468.6	0.23E+06	0.23E+06
0.223E+00	0.375E+00	1.20	32.	380.5	2.02	470.4	0.25E+06	0.25E+06
0.234E+00	0.375E+00	1.21	32.	379.5	2.01	472.5	0.26E+06	0.26E+06
0.245E+00	0.376E+00	1.22	32.	378.5	2.00	474.6	0.27E+06	0.27E+06
0.255E+00	0.377E+00	1.22	31.	377.7	1.99	476.4	0.28E+06	0.28E+06
0.266E+00	0.377E+00	1.23	31.	376.8	1.97	478.2	0.29E+06	0.29E+06
0.276E+00	0.378E+00	1.24	31.	375.8	1.96	480.3	0.30E+06	0.30E+06
0.287E+00	0.379E+00	1.24	30.	375.0	1.95	482.1	0.31E+06	0.31E+06
0.298E+00	0.380E+00	1.25	30.	374.1	1.94	483.8	0.33E+06	0.33E+06
0.308E+00	0.381E+00	1.25	30.	373.1	1.93	485.9	0.34E+06	0.34E+06
0.319E+00	0.382E+00	1.26	30.	372.3	1.92	487.7	0.35E+06	0.35E+06

File, WALLC.OUT - contains corrected wall coordinates

x(in)	yorg(in)	ycor(in)	d*x(in)	d*s(in)
0.0000E+00	0.3679E+00	0.3679E+00	0.0000E+00	0.0000E+00
0.1285E+00	0.3701E+00	0.3712E+00	0.5628E-03	0.5628E-03
0.1390E+00	0.3705E+00	0.3717E+00	0.5992E-03	0.5993E-03
0.1496E+00	0.3709E+00	0.3722E+00	0.6355E-03	0.6356E-03
0.1601E+00	0.3714E+00	0.3727E+00	0.6709E-03	0.6710E-03
0.1707E+00	0.3719E+00	0.3733E+00	0.7062E-03	0.7064E-03
0.1813E+00	0.3724E+00	0.3739E+00	0.7410E-03	0.7413E-03
0.1918E+00	0.3729E+00	0.3745E+00	0.7752E-03	0.7754E-03
0.2024E+00	0.3735E+00	0.3751E+00	0.8092E-03	0.8096E-03
0.2130E+00	0.3741E+00	0.3758E+00	0.8430E-03	0.8434E-03
0.2235E+00	0.3747E+00	0.3765E+00	0.8761E-03	0.8765E-03
0.2341E+00	0.3753E+00	0.3771E+00	0.9092E-03	0.9097E-03
0.2447E+00	0.3760E+00	0.3779E+00	0.9420E-03	0.9426E-03
0.2553E+00	0.3768E+00	0.3787E+00	0.9746E-03	0.9752E-03
0.2659E+00	0.3775E+00	0.3795E+00	0.1007E-02	0.1008E-02
0.2765E+00	0.3783E+00	0.3804E+00	0.1039E-02	0.1040E-02

0.2871E+00 0.3791E+00 0.3812E+00 0.1071E-02 0.1072E-02
 0.2977E+00 0.3799E+00 0.3821E+00 0.1102E-02 0.1103E-02
 0.3083E+00 0.3808E+00 0.3831E+00 0.1134E-02 0.1135E-02
 0.3189E+00 0.3817E+00 0.3840E+00 0.1165E-02 0.1166E-02
 0.3295E+00 0.3827E+00 0.3851E+00 0.1196E-02 0.1197E-02
 0.3401E+00 0.3836E+00 0.3861E+00 0.1227E-02 0.1228E-02
 0.3508E+00 0.3846E+00 0.3871E+00 0.1258E-02 0.1259E-02
 0.3614E+00 0.3857E+00 0.3883E+00 0.1288E-02 0.1290E-02
 0.3720E+00 0.3867E+00 0.3893E+00 0.1318E-02 0.1320E-02
 0.3827E+00 0.3878E+00 0.3905E+00 0.1349E-02 0.1351E-02
 0.3933E+00 0.3889E+00 0.3917E+00 0.1379E-02 0.1381E-02
 0.4040E+00 0.3901E+00 0.3929E+00 0.1409E-02 0.1411E-02
 0.4147E+00 0.3913E+00 0.3942E+00 0.1439E-02 0.1441E-02
 0.4341E+00 0.3935E+00 0.3965E+00 0.1492E-02 0.1495E-02
 0.6960E+00 0.4238E+00 0.4282E+00 0.2190E-02 0.2197E-02
 0.7256E+00 0.4272E+00 0.4317E+00 0.2265E-02 0.2273E-02
 0.7548E+00 0.4306E+00 0.4353E+00 0.2339E-02 0.2347E-02

Program WALL.FOR

Inputs: File, WALLC.OUT - output from BLCORR.FOR

Outputs: File, NOZ.TOP - contains x,y coordinates of subsonic and supersonic sections

x	y	
0.0000E+00	0.4184E+01	- First line of output data is beginning of converging section
0.2000E+01	0.4184E+01	
0.2092E+01	0.4179E+01	
0.2184E+01	0.4165E+01	
0.2276E+01	0.4143E+01	
0.2367E+01	0.4112E+01	
0.2459E+01	0.4073E+01	
0.2551E+01	0.4026E+01	
0.2643E+01	0.3973E+01	
0.2735E+01	0.3912E+01	
0.2827E+01	0.3845E+01	
0.2918E+01	0.3772E+01	
0.3010E+01	0.3693E+01	
0.3102E+01	0.3609E+01	
0.3194E+01	0.3521E+01	
0.3286E+01	0.3427E+01	
0.3378E+01	0.3330E+01	
0.3469E+01	0.3229E+01	
0.3561E+01	0.3125E+01	
0.3653E+01	0.3017E+01	
0.3745E+01	0.2908E+01	
0.3837E+01	0.2796E+01	
0.3929E+01	0.2682E+01	
0.4020E+01	0.2567E+01	
0.4112E+01	0.2451E+01	
0.4204E+01	0.2334E+01	

0.4296E+01	0.2218E+01
0.4388E+01	0.2101E+01
0.4480E+01	0.1985E+01
0.4571E+01	0.1870E+01
0.4663E+01	0.1756E+01
0.4755E+01	0.1644E+01
0.4847E+01	0.1534E+01
0.4939E+01	0.1427E+01
0.5031E+01	0.1323E+01
0.5122E+01	0.1222E+01
0.5214E+01	0.1124E+01
0.5306E+01	0.1031E+01
0.5398E+01	0.9424E+00
0.5490E+01	0.8585E+00
0.5582E+01	0.7798E+00
0.5673E+01	0.7068E+00
0.5765E+01	0.6398E+00
0.5857E+01	0.5793E+00
0.5949E+01	0.5255E+00
0.6041E+01	0.4790E+00
0.6133E+01	0.4400E+00
0.6224E+01	0.4091E+00
0.6316E+01	0.3865E+00
0.6408E+01	0.3726E+00
0.6500E+01	0.3679E+00
0.6639E+01	0.3717E+00
0.6660E+01	0.3727E+00
0.6681E+01	0.3739E+00
0.6702E+01	0.3751E+00
0.6723E+01	0.3765E+00
0.6745E+01	0.3779E+00
0.6766E+01	0.3795E+00
0.6787E+01	0.3812E+00
0.6808E+01	0.3831E+00

- Throat - Previously corrected diverging section follows from here

File, NOZ.BOT - contains x,y coordinates of subsonic and supersonic sections if bottom wall was straight
 Output has same general format with slight differences. File not really useful unless constructing only one half a nozzle.

x	y
0.0000E+00	-0.3816E+01
0.2000E+01	-0.3816E+01
0.2092E+01	-0.3811E+01
0.2184E+01	-0.3797E+01
0.2276E+01	-0.3775E+01
0.2367E+01	-0.3744E+01
0.2459E+01	-0.3705E+01
0.2551E+01	-0.3658E+01
0.2643E+01	-0.3605E+01
0.2735E+01	-0.3544E+01

Program BLOWDOT.FOR

Inputs: File, BLOWIN.DAT

HE8 1.39 70.71 485.0918 14.276 71.7 29.067 1.886
HE9 1.39 70.71 485.0918 14.276 71.8 29.067 1.886
HE10 1.39 69.255 475.1057 14.276 71.6 29.067 1.886
TIME1 1.39 69.983 480.0988 14.295 71.7 29.105 1.886
TIME2 1.39 69.983 480.0988 14.295 71.7 29.105 1.886
TIME3 1.39 69.983 480.0988 14.295 71.7 29.105 1.886
BLOW2 1.39 69.983 480.0988 37.352 290.15 29.2 1.884
BLOW4 1.39 69.983 480.0988 37.617 293.2611 29.2 1.884
BLOW5 1.39 69.983 480.0988 37.737 290.65 28.985 1.884
BLOW6 1.39 69.983 480.0988 37.799 292.0944 28.988 1.884
1MID2 1.39 69.983 480.0988 45.431 288.7056 29.125 1.86
1MID3 1.39 69.983 480.0988 45.513 288.7056 29.125 1.86
1MID4 1.39 69.983 480.0988 45.529 289.2611 29.12 1.86
1MID5 1.39 69.983 480.0988 45.658 288.15 29.12 1.86
1MID6 1.39 69.983 480.0988 45.721 288.2611 29.12 1.86
2MID1 1.39 69.983 480.0988 50.805 287.5944 29.12 1.862
2MID2 1.39 69.983 480.0988 50.869 287.8722 29.12 1.862
MAX1 1.39 69.983 480.0988 55.44 289.8722 29.037 1.848
MAX2 1.39 69.983 480.0988 55.352 287.7056 29.045 1.848
MAX3 1.39 69.983 480.0988 55.042 288.0944 29.045 1.848
MAX4 1.39 69.983 480.0988 55.607 288.2611 29.045 1.848
MAX5 1.39 69.983 480.0988 49.996 287.3722 29.045 1.848

Format: File Name, γ , chamber pressure (psi), chamber temperature (K), plenum pressure (psi), plenum temperature (F or K), atmospheric pressure (in Hg), exit Mach number

Outputs: File, BLOWRAT.OUT

Test Conditions:

Run:HE8

Gamma = 1.3900
Pa = 14.2764 psi
P0 = 70.7100 psi
T0 = 485.0918 K
Ppl = 14.2760 psi
Tpl = 295.2056 K

Initial Calculations:

mdotinf = 1.6946 kg/sec
RHOUinf = 892.4648 kg/m²-s
rhojinj = 1.1618 kg/m³

Heat Flux Gauge Blowing Ratios:

B(1) = 0.000000
B(2) = 0.000000
B(3) = 0.000028

Total Blowing Ratio Calculations:

lsum = 1.099075 m

RHOUsu = 0.000144 kg/m²-s

BT = 0.000131

Performance Calculations:

Pos mdot = 0.000157 kg/sec

Neg mdot = -.003254 kg/sec

Tot mdot 1.6915 kg/sec

Pe = 10.7833 psi

Te = 286.2008 K

ue = 637.2729 m/s

Thrust = 998.48 N

Isp = 60.1711 sec

***** Program BLOWDOT calculates the total mass flow through the porous material for given test conditions. Blowing ratios are calculated in one manner which will be indicated for heat flux purposes, and another way (the Keener #, which will be indicated) for performance purposes. The program performs a

***** summation of surface length and mass flow rate along the porous surface at intervals*****
***** defined by the coordinates of the model in the blowing ratio calculation.

***** Author: 2Lt David N. Keener 513-255-3636 x1249

***** Date: September 1994

PROGRAM BLOWDOT

IMPLICIT NONE

```
REAL*8 rhoij,Ppl,R,Tpl,uinj,ainj,SA,mdot,mdotinf,B(3),BT,Knum
REAL*8 mdotsum,CF,P,Astar,in2msq,RHOUinf,P0,T0,psi2Pa,linj
REAL*8 M(54),x(54),y(54),GAMMA,xsa,Aexit,RHOUinj,RHOUsu,lsum
```

INTEGER*4 i

CHARACTER*8 NAME

```
OPEN(1,'c:\qed\data\isentrop.dat')
OPEN(2,'c:\qed\data\blowin.dat')
OPEN(3,'c:\qed\data\blowrat.out')
OPEN(4,'c:\qed\data\plotmdot.out')
```

***** Variable and Output File Initialization *****

```
write(3,*) 'Blowing Ratios at each heat flux gauge and Total Blo  
cwing Ratio'  
write(3,*)  
write(3,*) 'Test Conditions.'  
write(4,*) 'Mass flow data at each interval'  
write(4,*)  
write(4,*) 'Test Conditions.'  
SA=0.0D0  
mdot=0.0D0  
mdotsum=0.0D0  
lsum=0.0D0  
RHOUsum=0.0D0  
DO I=1,3  
    B(i) = 0.0D0  
ENDDO  
BT=0.0D0
```

***** Constants *****

R = 287.0D0	!J/(kg-K)!
in2msq = .00064516D0	
psi2Pa = 6894.7572D0	
Astar = .3679D0*8.0D0*in2msq	!m^2!
Aexit = .6395D0*8.0D0*in2msq	!m^2!

***** Read in data needed for problem *****

```
DO i=1,54  
    READ(1,*) x(i),y(i),M(i)  
ENDDO  
READ(2,*) NAME,GAMMA,P0,T0,Ppl,Tpl !pressure in psi!
```

***** Convert plenum temperature to Kelvin if it is not input that way *****

```
IF (Tpl .lt. 100.0D0) THEN  
    Tpl = (Tpl+459.67D0)/1.8D0  
ENDIF  
write(3,*) 'Run:',NAME  
write(3,*)  
write(3,30) 'Gamma =' ,GAMMA  
write(3,31) 'P0 =' ,P0  
write(3,32) 'T0 =' ,T0  
write(3,31) 'Ppl =' ,Ppl  
write(3,32) 'Tpl =' ,Tpl  
write(4,30) 'Gamma =' ,GAMMA  
write(4,31) 'P0 =' ,P0
```

```

write(4,32) 'T0    =' ,T0
write(4,31) 'Ppl   =' ,Ppl
write(4,32) 'Tpl   =' ,Tpl
P0 = P0*psi2Pa
Ppl = Ppl*psi2Pa

***** Initial calculations for iteration *****
write(3,*)
write(3,* ) 'Initial Calculations:'
write(4,*)
write(4,* ) 'Initial Calculations:'
mdotinf=DSQRT(GAMMA/(R*T0)*((2.0D0/(GAMMA+1.0D0))**2
c      ((GAMMA+1.0D0)/(GAMMA-1.0D0)))*Astar*P0      !kg/sec!
write(3,30) 'mdotinf =' ,mdotinf
write(4,30) 'mdotinf =' ,mdotinf
RHOUinf=mdotinf/Astar                         !kg/(m^2-sec) !
write(3,30) 'RHOUinf =' ,RHOUinf
write(4,30) 'RHOUinf =' ,RHOUinf
rhoanj=Ppl/(R*Tpl)                            !kg/m^3 !
write(3,30) 'rhoanj  =' ,rhoanj
write(4,30) 'rhoanj  =' ,rhoanj
write(3,*)
write(4,*)
write(4,40)

```

***** Begin summation iteration. For this experiment only 53 points were needed
***** along the nozzle. This can be changed appropriately.

DO i=2,53

***** Correction factors were fit to correct isentropic predictions from original design to *****
***** to measured data to increase accuracy of blowing ratios.

```

IF (M(i) .lt. 1.6919D0) THEN
  CF=0.0155*M(i)**3.0D0 + 0.9722D0
ENDIF
IF (M(i) .ge. 1.6919D0) THEN
  CF=0.0132*M(i)**6.0D0 - 0.0356*M(i)**4.0D0 + 1.0302
ENDIF
P=P0/((1.0D0+(GAMMA-1.0D0)/2.0D0*M(i)**2.0D0)**(GAMMA/
c      (GAMMA-1.0D0)))*CF                      !Pa!

```

***** Delta P across porous material because there are four layers of
***** material between plenum and nozzle wall

```

uinj=(DABS(((Ppl/psi2Pa)-(P/psi2Pa))/4.0D0)/.03243D0)**2
c      (1.0D0/.9585D0)*.3048D0/60.0D0          !m/s!
IF ((Ppl - P) .lt. 0.0D0) THEN

```

```

        uinj = uinj*(-1.0D0)
        ENDIF
        linj=DSQRT(((x(i+1)+x(i))/2-(x(i)+x(i-1))/2)**2.0D0) +
c          (((y(i+1)+y(i))/2-(y(i)+y(i-1))/2)**2.0D0))
        ainj=linj*3.0D0*in2msq                                !m^2!
        RHOUinj = rho*uinj
        mdot=RHOUinj*ainj                                    !kg/sec!
        IF (i .eq. 11) THEN
            xsa = (y(i) + .7976D0 * (y(i+1)-y(i))) * 8.0D0 * in2msq
            B(1) = ((mdotsum + .2853D0*mdot)/(SA + .2853D0*ainj))/
c              (mdotinf/xsa)
            IF (B(1) .lt. 0.0D0) THEN
                B(1) = 0.0D0
            ENDIF
            write(*,*) 'Writing Blowing Ratio 1 to file'
            WRITE(3,20) 'B(1) =',B(1)
        ENDIF
        IF (i .eq. 23) THEN
            xsa = (y(i+1) + .7976D0 * (y(i+2)-y(i+1))) * 8.0D0 *
c              in2msq
            B(2) = ((mdotsum + .7828D0*mdot)/(SA + .7828D0*ainj))/
c              (mdotinf/xsa)
            IF (B(2) .lt. 0.0D0) THEN
                B(2) = 0.0D0
            ENDIF
            write(*,*) 'Writing Blowing Ratio 2 to file'
            WRITE(3,20) 'B(2) =',B(2)
        ENDIF
        IF (i .eq. 47) THEN
            xsa = (y(i) + .7976D0 * (y(i+1)-y(i))) * 8.0D0 * in2msq
            B(3) = ((mdotsum + .1201D0*mdot)/(SA + .1201D0*ainj))/
c              (mdotinf/xsa)
            IF (B(3) .lt. 0.0D0) THEN
                B(3) = 0.0D0
            ENDIF
            write(*,*) 'Writing Blowing Ratio 3 to file'
            WRITE(3,20) 'B(3) =',B(3)
        ENDIF
        lsum=lsum+linj
        RHOUsu=RHOUsum+(RHOUinj/(mdotinf/(y(i)*8.0D0*in2msq)))*
c          linj
        SA=ainj+SA                                !m^2!
        mdotsum=mdot+mdotsum                      !kg/sec!
        IF (mdotsum .le. 0.0D0) THEN
            mdotsum = 0.0D0

```

```

lsum=0.0D0
RHOUsu=0.0D0
ENDIF
write(4,10) (i-1),x(i),CF,(P/psi2Pa),mdot,mdotsum
ENDDO
BT = (mdotsum/SA)/(mdotinf/Aexit)
c BTavg = (mdotsum/SA)/(RHOUsu/lsum)
Knum = RHOUsu/lsum
WRITE(3,20) 'BT =',BT
WRITE(3,50) 'Keener # =',Knum
c WRITE(3,50) 'lsum =',lsum
c WRITE(3,50) 'RHOUsu =',RHOUsu
STOP
10 format(I2,3X,F6.4,3X,F6.4,3X,F5.2,3X,F10.8,3X,F10.8)
20 format(A7,F8.6)
30 format(A9,F8.4)
31 format(A9,F8.4,' psi')
32 format(A9,F8.4,' K')
40 format(8X,'x',7X,'CF',7X,'P',9X,'mdot',7X,'mdotsum')
50 format(A10,F10.6)
END

```

APPENDIX C
Calibration Data

C.1

<u>Number</u>	<u>Serial Number</u>	<u>Location</u>	<u>Slope</u>
1	WB80	Tube 1	0.15838
2	44AM	Tube 2	0.14378
3	SNJ82P	Plenum	0.01836
4	TM73	Non Blowing 1	0.06754
5	29BA	Converging Section	0.02640
6	TM83	Blowing 1	0.06895
7	TN05	Blowing 2	0.05519
8	TN04	Blowing 3	0.07007
9	WL43	Non Blowing 2	0.05073
10	39BP	Non Blowing 3	0.05344
Pitot			0.11203

Very high confidence was placed on these calibrations because the maximum error from a linear best fit in any of these transducers was 0.485% of the standard deviation in the data. Therefore, it is unlikely that error in any of the pressure data presented here was due to calibration error.

APPENDIX D

Procedures

D.1

Shock Tube Run Procedure - Helium Driver w/ Shadowgraph

**** NOTE:** If running open-air shock, make sure **EVERYONE IN ROOM IS WEARING EAR PROTECTION!!!!**

**** NOTE:** When taking shadowgraphs, as many possible light sources must be eliminated from the room including computer monitors.

**** NOTE:** Before starting a test including shadowgraphs, turn out all room lights except those controlled by the switch near the tube controls.

1. With tube closed, open air valve and "P4."
2. Allow house air to run through the tube for 5 minutes to purge any excess helium from previous runs or any stagnant ambient air.

During the purge period:

3. Load film cartridge into film holder.
4. Load film holder into camera.
5. Reset Model 436 Proportional Delay Generator and Model 453 Delay Generator.

When purge period is complete:

6. Close air valve and "P4."
7. Open tube and remove spent mylar diaphragm.
8. Reset plunger.
9. Close and secure tube with hydraulic jack.
10. Open helium bottle and ball valve.
11. Select "One Shot" on Nicolet system.
12. Turn down brightness on computer monitor.
13. Open "Plunger" valve and verify pressure to plunger.
14. Open "P4 Gauge."
15. Slowly open "P4." P4 must be increasing at a slow rate.

16. Turn out remaining room lights.
17. Expose film.
18. Allow pressure to rise in driver to desired pressure then close "P4."
19. Repeatedly open and close "P4" until driver settles at desired pressure.
20. Verify no personnel standing near exit of shock tube and PhD students in room are aware of
impending test.
21. Initiate test by depressing the plunger arm.
22. Relieve excess plunger pressure by opening "Plunger Bleed."
23. Relieve excess driver pressure by opening "P4 Bleed."
24. Close helium bottle and ball valve.
25. Close film cartridge and begin image developing.
26. Turn on room lights.

Shock Tube Procedure - Air Only Driver

**** NOTE:** If running open-air shock, make sure **EVERYONE IN ROOM IS WEARING EAR PROTECTION!!!!**

1. Close "Plunger" valve and "P4" valve.
2. Open "Plunger Bleed" and "P4 Bleed."
3. Reset plunger.
4. Close "Plunger Bleed" and "P4 Bleed."
5. Load shock tube with appropriate thickness mylar diaphragm.
6. Open "Plunger" valve and verify pressure to plunger.
7. Open "P4 Gauge."
8. Slowly open "P4."
9. Select "One Shot" on Nicolet system.
10. Allow pressure to rise in driver to desired pressure then close "P4."
11. Open and close "P4" until driver settles at desired pressure.
12. Verify no personnel standing near exit of shock tube and PhD students in room are aware of impending test.
13. Run shock by depressing plunger arm.
14. Open shock tube and remove spent mylar.

APPENDIX E

Throat Boundary Layer Thickness Calculation

E.1

Discharge Coefficient:

$$C_D = 1 - \left(\frac{\gamma + 1}{2} \right)^{\frac{3}{4}} \left\{ \frac{-2.128}{\gamma + 1} + 3.266 \right\} R^{-\frac{1}{2}} + 0.9428 \frac{(\gamma - 1)(\gamma + 2)}{(\gamma + 1)^{\frac{1}{2}}} R^{-1} \quad (2-13)$$

$$R = \text{Re}^* \left(\frac{R^*}{R_c} \right)^{\frac{1}{2}} \quad (2-14)$$

where: γ = ratio of specific heats (c_p/c_v) = 1.39

Re^* = Reynolds number at the throat

R^* = throat radius = 9.34466×10^{-3} m

R_c = radius of curvature of the throat = $0.9'' = .02286$ m

R = constant used to calculate discharge coefficient

The only other quantity necessary to solve Eq.2-14 is Re^* , which is given by Eq.E-1.

$$\text{Re}^* = \frac{\rho^* u^* D^*}{\mu^*} \quad (\text{E-1})$$

where: ρ^* = density of gas at the throat (kg/m³)

u^* = velocity of gas at the throat (m/s)

D^* = diameter of the throat (m) = 1.868932×10^{-2} m

μ^* = viscosity at the throat (N-s/m²) = 229.4×10^{-7} N-s/m² (Hill and Peterson, 694)

Representative chamber conditions were taken to be: 477 kPa (69.24 psi)

475 K

By isentropic relations, throat conditions were: 253 kPa (36.69 psi)

397.49 K

E.2

Therefore, because

$$\rho^* = \frac{p^*}{RT^*}$$
$$u^* = \sqrt{(\gamma \cdot R \cdot T^*)}$$

at the throat,

$$\rho^* = 2.21718 \text{ kg/m}^3$$

$$u^* = 398.208 \text{ m/s}$$

and

$$Re^* = 719,303.615.$$

It follows, then, from Eqs. 2-13 and 2-14 that $R = 4.83605 \times 10^5$ and $C_D = .996097$. Using Eq. 2-15, δ_t is calculated to be **0.0182 mm (0.0007179")**.

$$\frac{\delta_t}{R^*} = \frac{1 - C_D}{2} \quad (2-15)$$

This value was calculated because the boundary layer was not measurable near the throat from shadowgraphs because it was so thin there. This value was used as a data point in this report when boundary layer at the throat was plotted or quoted because it was known that the boundary layer did exist at the throat, and this is a good estimate of its thickness.

APPENDIX F
Selecting a Porous Material

F.1

The porous material used in this experiment was chosen based on strength mass flow rate considerations. The pressure the material was required to hold was the major factor in choosing the type of metal used, and the desired mass flow rate through the material determined the porosity chosen. Mott Metallurgical Company was identified as the source of the material, and analysis was accomplished based on strength and mass flow data provided by Mott.

Strength Analysis

Design plenum pressure: 552 kPa (80 psi)

Maximum plenum pressure: 690 kPa (100 psi) (defined by the limit of the pressure transducers)

Blowing area: 58 cm²

Maximum pressure force on the porous material: 4 kN

Maximum pressure on porous area: 690 kPa

Pressure limit of 316L sintered stainless steel: 53MPa

The 316L sintered stainless steel was the least strong material available, and the pressure shown above was material with the greatest porosity available. Therefore, 316L stainless steel was more than adequate to withstand the expected pressure force, and this material was selected as the type of porous material, but porosity grade also had to be selected.

Mass Flow Analysis

The porosity grade depended on the desired mass flow through the porous material. Mott Metallurgical manufactured their material in 1.57 mm (.062") thick sheets, and in order to mount pressure transducers and heat flux gauges properly four sheets of material were used. Mass flow through porous material is related to the pressure drop across the material, and since all mass flow data provided by Mott was quoted for one layer, all pressure drops in the following calculations had to be divided by four to take each layer into account. Arbitrarily, the desired blowing ratios were chosen to be 0.01 and 0.05 at the throat.

Predicted chamber conditions: 538 kPa (78 psi)

491 K

and isentropic relations allowed calculation of $\rho^* u^*$ (where * indicates the throat).

The injection parameter, $\rho_i u_i$, is then calculated by Eq.F-1.

$$\rho_i u_i = B \cdot (\rho^* u^*) \quad (\text{F-1})$$

where: B = blowing ratio

ρ = gas density (kg/m³)

u = gas velocity (m/s)

Pressure to the plenum was provided with bottled air.

Assumed bottle conditions: 13.8 MPa (2000 psi)

297 K

Plenum temperature (from Mollier diagram for nitrogen at constant enthalpy): 272 K

Using the estimated plenum temperature, the plenum pressure, and the perfect gas law, ρ_p was calculated. Assuming that $\rho_i = \rho_p$ because the porous material was thin, u_i was calculated. From a log-log chart relating mass flow to pressure drop provided by Mott (see Fig F.1), equations of the form (F-2) were created.

$$\Delta p = A u_i^B \quad (F-2)$$

where: Δp = pressure drop (psi)

A, B = constants determined from the chart

u_i = injection velocity (ft/min)

Inserting the design pressure drop and injection velocity in the correct units into Eq.F-2 determined that 2 micron porosity was suited for $B=0.01$ and 10 micron porosity was suited for $B=0.05$. In reality, only the 2 micron porosity material was used, and this analysis was validated to within 2% of Mott data.

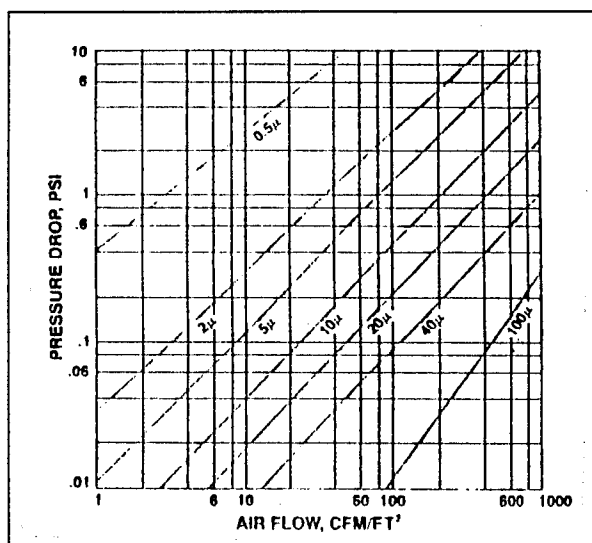


Figure F.1 - Mass Flow vs Pressure Drop (Mott)

Vita

2Lt David N. Keener was born on 15 December 1970 in Elyria, Ohio, and is the son of Nelson E. and Diana J. Keener of New Palestine, Indiana. He has one brother, Craig. He graduated from Midview High School in Grafton, Ohio in 1989, and entered the United States Air Force Academy. Upon graduation in 1993, he received his regular commission and Bachelor of Science Degree in Astronautical Engineering. He entered the School of Engineering, Air Force Institute of Technology, in June 1993, and upon graduation will be assigned to the Phillips Laboratory, Kirtland AFB, NM.

Permanent Address: 2784 High Acres West, New Palestine, IN 46431

REPORT DOCUMENTATION PAGE

Form Approved
OMB No. 0704-0188

Public reporting burden for this collection of information is estimated to average 1 hour per response, including the time for reviewing instructions, searching existing data sources, gathering and maintaining the data needed, and completing and reviewing the collection of information. Send comments regarding this burden estimate or any other aspect of this collection of information, including suggestions for reducing this burden, to Washington Headquarters Services, Directorate for Information Operations and Reports, 1215 Jefferson Davis Highway, Suite 1204, Arlington, VA 22202-4302, and to the Office of Management and Budget, Paperwork Reduction Project (0704-0188), Washington, DC 20503.

1. AGENCY USE ONLY (Leave blank)			2. REPORT DATE		3. REPORT TYPE AND DATES COVERED		
			December 1994		Master's Thesis		
4. TITLE AND SUBTITLE INVESTIGATION OF BOUNDARY LAYER AND PERFORMANCE EFFECTS OF TRANSPERSION COOLING THROUGH A POROUS PLATE IN A ROCKET NOZZLE					5. FUNDING NUMBERS		
6. AUTHOR(S) David N. Keener, 2Lt., USAF							
7. PERFORMING ORGANIZATION NAME(S) AND ADDRESS(ES) Air Force Institute of Technology, WPAFB, OH 45433-6583					8. PERFORMING ORGANIZATION REPORT NUMBER AFIT/GA/ENY/94D-3		
9. SPONSORING / MONITORING AGENCY NAME(S) AND ADDRESS(ES) Mr. Terrance Galati Phillips Lab					10. SPONSORING / MONITORING AGENCY REPORT NUMBER OLAC PL/RKCA, 4 Draco Dr. Edwards AFB, CA 93524-7190		
11. SUPPLEMENTARY NOTES							
12a. DISTRIBUTION / AVAILABILITY STATEMENT Approved for public release; distribution unlimited				12b. DISTRIBUTION CODE			
13. ABSTRACT (Maximum 200 words) This study used a range of low blowing ratios with air through an area of porous material in a Mach 2.0 nozzle to quantify the change in boundary layer thickness as a function of blowing ratio. Also, exit and wall Mach number profiles at each blowing ratio were collected to characterize performance losses as a result of blowing. Performance in terms of specific impulse was also studied. As expected, the boundary layer thickness increased and nozzle performance in terms of exit Mach number decreased with increasing blowing ratio.							
14. SUBJECT TERMS Porous Material, Boundary Layer, Transpiration Cooling, Shock Tunnel, Heat Transfer, Performance, Blowing Rocket Nozzle, Pressure Gradient					15. NUMBER OF PAGES 114		
					16. PRICE CODE 16		
17. SECURITY CLASSIFICATION OF REPORT Unclassified		18. SECURITY CLASSIFICATION OF THIS PAGE Unclassified		19. SECURITY CLASSIFICATION OF ABSTRACT Unclassified		20. LIMITATION OF ABSTRACT UL	